Stratigraphic record of basin development within the San Andreas fault system: Late Cenozoic Fish Creek–Vallecito basin, southern California

Rebecca J. Dorsey[1†], Bernard A. Housen[2], Susanne U. Janecke[3], C. Mark Fanning[4], and Amy L.F. Spears[2]
[1]*Department of Geological Sciences, 1272 University of Oregon, Eugene, Oregon 97403-1272, USA*
[2]*Department of Geology (ES 236), Western Washington University, 516 High Street, Bellingham, Washington 98225-9080, USA*
[3]*Department of Geology, Utah State University, 4505 Old Main Hill, Logan, Utah 84322-4505, USA*
[4]*Research School of Earth Sciences, Australian National University, Building 61, Mills Road, Canberra, ACT 0200, Australia*

ABSTRACT

The Fish Creek–Vallecito basin contains a 5.5-km-thick section of late Miocene to early Pleistocene sedimentary rocks exposed in the hanging wall of the West Salton detachment fault. These deposits preserve a high-fidelity record of late Cenozoic subsidence and basin filling that resulted from deformation in the San Andreas fault system of southern California. Existing and new paleomagnetic data, combined with new U-Pb zircon ages of two tuffs high in the section, show that the section ranges in age from ca. 8.0 ± 0.4 Ma at the base to ca. 0.95 Ma at the top. Geohistory analysis reveals: (1) moderate subsidence (0.46 mm/yr) from ca. 8.0 to 4.5 Ma; (2) rapid subsidence (2.1 mm/yr) from 4.5 to 3.1 Ma; (3) moderate subsidence (0.40 mm/yr) from 3.1 to 0.95 Ma; and (4) rapid uplift and erosion that has exhumed the section since ca. 1 Ma. Onset of sedimentation at ca. 8.0 ± 0.4 Ma records earliest extension or transtension in the area, possibly related to localization of the Pacific–North America plate boundary in the Salton Trough and Gulf of California. Alternatively, marine incursion at 6.3 Ma may be the earliest record of plate-boundary deformation in the Gulf of California–Salton Trough region. A thick interval higher in the section records progradation of the Colorado River delta into and across the basin starting ca. 4.9 Ma. Progradation continued during an abrupt increase in subsidence rate at 4.5 Ma, and fluvial-deltaic conditions persisted for 1.4 m.y. during the rapid-subsidence phase, indicating that delta progradation was driven by a large increase in rate of sediment input from the Colorado River. Uplift and inversion of the basin starting ca. 1.0 Ma record initiation of strike-slip faults that define the modern phase of dextral wrench tectonics in the western Salton Trough.

INTRODUCTION

Sedimentary basins that form adjacent to transform faults offer unique insights into regional isostasy, strain partitioning, fault displacements, and kinematic evolution of strike-slip fault zones (e.g., Mann et al., 1983; Christie-Blick and Biddle, 1985; May et al., 1993; Crowell, 2003; Mann, 2007; Seeber et al., 2010). Stratigraphic studies allow us to track the initiation and development of continental transforms because motion on strike-slip faults typically produces local- to regional-scale crustal subsidence that leads to accumulation and preservation of sedimentary deposits. The Salton Trough in southern California is a large, late Cenozoic transform basin at the northwest end of the Gulf of California (Fig. 1) that has subsided and filled in response to changes in crustal thickness, sediment input, and deformation associated with development of the San Andreas fault. While it is well known that transtensional deformation resulted in deep subsidence and basin filling during Miocene to Pleistocene time (Dibblee, 1954, 1984; Johnson et al., 1983; Winker, 1987; Herzig et al., 1988; Winker and Kidwell, 1996), the timing of basin initiation, changes in subsidence rate, and relation to the kinematic evolution of the Pacific–North America plate boundary are incompletely understood.

A thick stratigraphic record is exposed in the western Salton Trough, where dextral wrench deformation has resulted in rapid uplift and erosion of late Cenozoic deposits since ca. 1.1–1.3 Ma (Figs. 1 and 2; Steely et al., 2009; Janecke et al., 2010). These sedimentary rocks contain a rich record of basin subsidence, sediment accumulation, delta progradation, and changing patterns of crustal deformation since late Miocene time. During much of the basin's history, regional strain and crustal subsidence were accommodated by combined slip on the low-angle West Salton detachment fault in the west and the San Andreas transform fault on the northeast side of the basin (Axen and Fletcher, 1998). Despite this general understanding, the age of the West Salton detachment fault is poorly known; it could have initiated as early as ca. 12 Ma (Shirvell et al., 2009) or as late as earliest Pliocene (Steely, 2006). Moreover, the timing of initiation of the San Andreas fault system in the Salton Trough and Gulf of California region is uncertain, with estimates ranging from 12 to 17 Ma (e.g., Powell and Weldon, 1992; Matti and Morton, 1993; Gans, 1997; Fletcher et al., 2007) to ca. 6 Ma (e.g., Stock and Hodges, 1989; Nicholson et al., 1994; Ingersoll and Rumelhart, 1999; Atwater and Stock, 1998; Oskin and Stock, 2003b). Lack of consensus on these questions currently obscures our understanding of the kinematic evolution of the Pacific–North America plate boundary through time.

In addition to regional deformation, voluminous input of sediment from the Colorado River has exerted a major influence on late Cenozoic paleogeography and crustal evolution in the Salton Trough and northern Gulf of California. Colorado River sediment is rapidly buried and metamorphosed in active basins, where it is mixed with mantle-derived intrusions and converted to young metamorphic rock (Muffler and White, 1969; Fuis et al., 1984; Elders

[†]E-mail: rdorsey@uoregon.edu

GSA Bulletin; May/June 2011; v. 123; no. 5/6; p. 771–793; doi: 10.1130/B30168.1; 14 figures; 1 table; Data Repository item 2010211.

and Sass, 1988; Schmitt and Vazquez, 2006). The volume of sediment in the basins is roughly equal to material eroded from the Colorado Plateau in the past 5–6 m.y., and it contributes to crustal growth along the plate boundary at rates similar to those documented for subduction-related magmatic arcs and seafloor spreading centers (Dorsey, 2010). Although input of sediment clearly affects thermal structure, crustal rheology, and deformation style in this setting (Persaud et al., 2003; González-Fernández et al., 2005; Lizarralde et al., 2007; Bialas and Buck, 2009; Dorsey and Umhoefer, 2010), little is known about the interplay between crustal subsidence and Pliocene progradation of the Colorado River delta into and across the Salton Trough basin.

This paper presents the results of an integrated field, stratigraphic, paleomagnetic, and geohistory analysis of the Fish Creek–Vallecito basin in the western Salton Trough (Fig. 1). Previous studies have provided insights into the age, lithology, depositional environments, and subsidence history, while also leaving some problems unresolved. Magnetostratigraphic studies (Opdyke et al., 1977; Johnson et al., 1983) started ~1000 m above the base of the section, thus omitting the first ~3.2 m.y. (~45%) of the basin history. Winker (1987) analyzed geologic structures, depositional environments, paleocurrents, and basin architecture, but relied on existing age controls to interpret the basin history and did not recognize the significant role of the basin-bounding West Salton detachment fault. In this study, we use new detailed geologic mapping, section measuring, and paleomagnetic analyses to document a continuous section that passes through an area of newly recognized structural complexity, thus permitting quantitative geohistory analysis of the entire 5.5-km-thick basinal succession. When integrated with prior studies, the new data allow us to test hypotheses for the timing of plate-boundary–related crustal deformation and dynamic controls on progradation of the Colorado River delta.

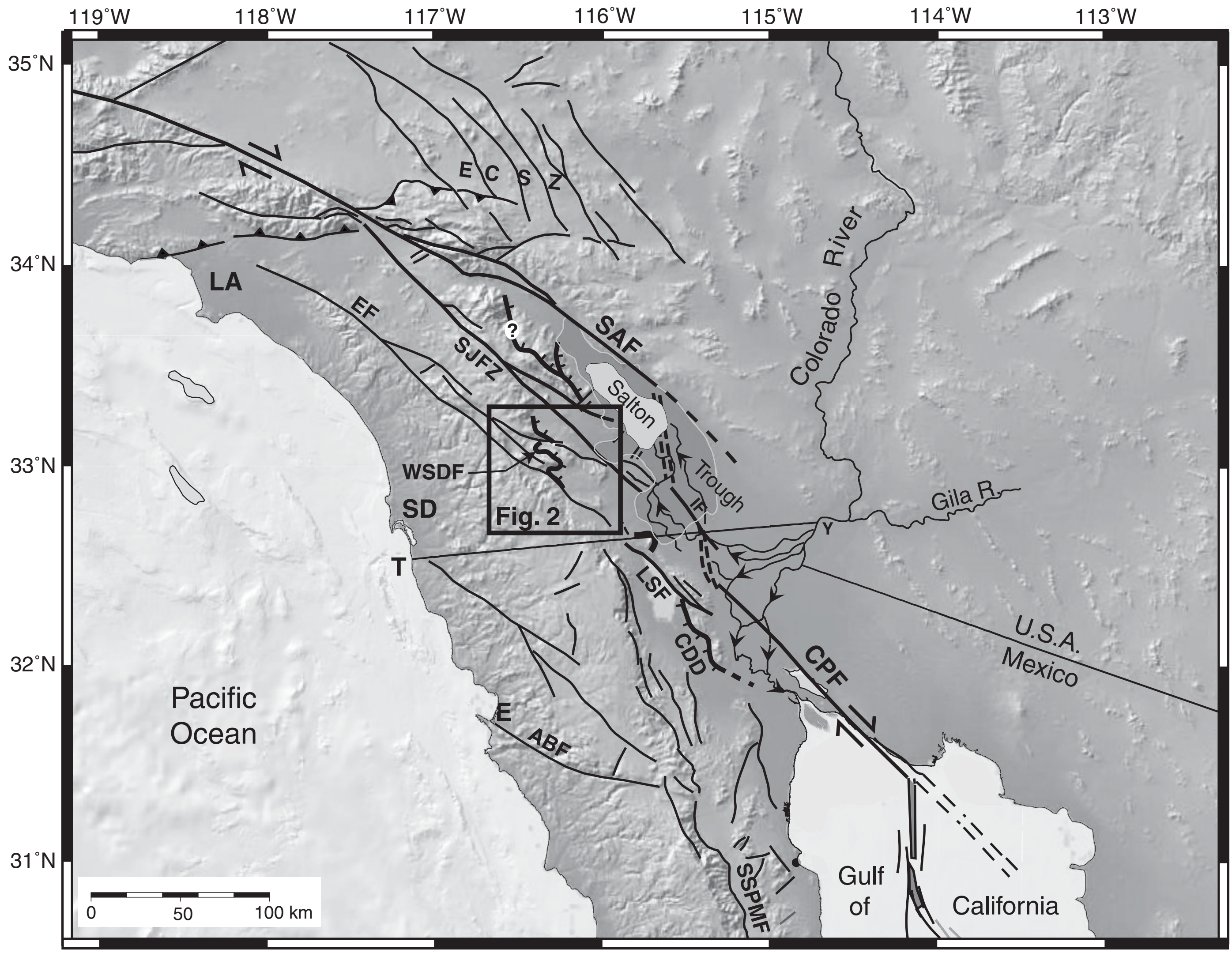

Figure 1. Regional map of topography and main faults of the San Andreas fault system in the southwestern United States and northwestern Mexico. The Salton Trough is a large transtensional basin that straddles the Pacific–North America plate boundary in southern California. ABF—Agua Blanca fault; CDD—Canada David detachment; CPF—Cerro Prieto fault; E—Ensenada; ECSZ—eastern California shear zone; EF—Elsinore fault; IF—Imperial fault; LA—Los Angeles; LSF—Laguna Salada fault; SAF—San Andreas fault; SD—San Diego; SJFZ—San Jacinto fault zone; SSPMF—Sierra San Pedro Martir fault; T—Tijuana; WSDF—West Salton detachment fault; Y—Yuma.

TECTONIC SETTING AND STRATIGRAPHY

Salton Trough Region

The Fish Creek–Vallecito basin is part of a large, late Cenozoic sedimentary basin that formed in the hanging wall of the West Salton detachment fault and was bounded on the northeast side of the Salton Trough by the San Andreas fault (Fig. 1; Dibblee, 1954, 1984; Axen and Fletcher, 1998; Dorsey, 2006). Regional extension, transtension, and crustal subsidence led to late Miocene deposition of coarse clastic alluvial deposits and overlying marine turbidites, followed by Pliocene to early Pleistocene subsidence and filling of the Salton Trough basin with marine and nonmarine deposits (Dibblee, 1954, 1984; Woodard, 1963, 1974; Kerr, 1982; Winker, 1987; Kerr and Kidwell, 1991; Dibblee, 1996; Winker and Kidwell, 1996;

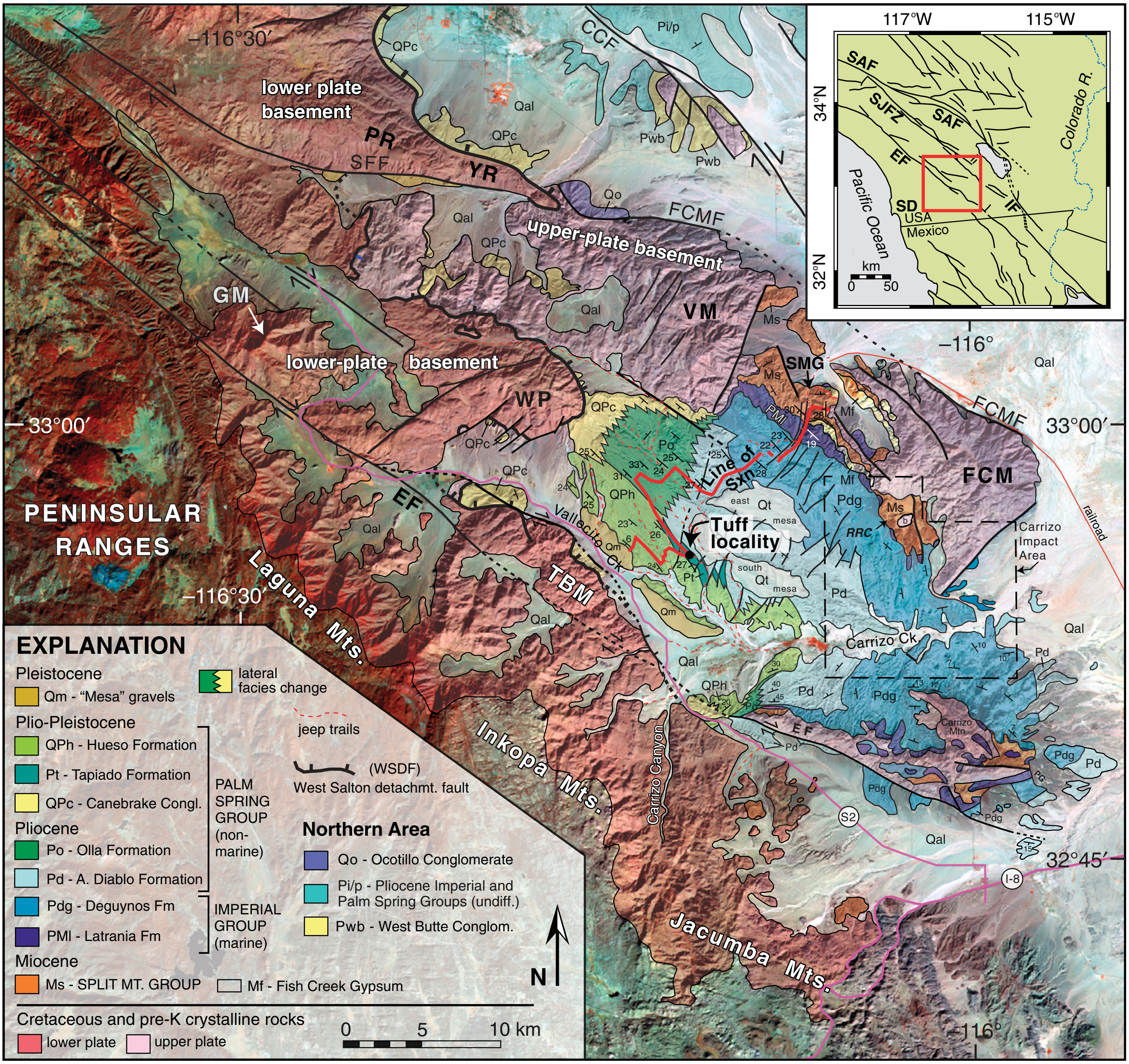

Figure 2. Geologic map of the Fish Creek–Vallecito basin and surrounding area, modified from Winker (1987), Winker and Kidwell (1996), Dibblee (1996), Axen and Fletcher (1998), Kairouz (2005), G. Axen (2008, personal commun.), and Steely (2006). CCF—Coyote Creek fault; FCM—Fish Creek Mountains; FCMF—Fish Creek Mountains fault; GM—Granite Mountain; PR—Pinyon Ridge; RRC—Red Rock Canyon; SFF—San Felipe fault; SMG—Split Mountain Gorge; TBM—Tierra Blanca Mountains; VM—Vallecito Mountains; YR—Yaqui Ridge; WP—Whale Peak.

Axen and Fletcher, 1998; Dorsey et al., 2007; McDougall, 2008). Colorado River sediment constructed a large delta that prograded into marine water and filled the basin at the north end of the Gulf of California during Pliocene time, when the Fish Creek–Vallecito basin was contiguous with the larger Salton Trough depocenter (Winker and Kidwell, 1986). Sediment derived from local basement uplifts, including the footwall of the West Salton detachment fault, produced coarse arkosic Pliocene-Pleistocene conglomerate and sandstone that interfinger laterally with Colorado River sediment and make up a narrow belt of coarse alluvial facies around the margins of the basin (Winker and Kidwell, 1996; Kairouz, 2005; Steely, 2006; Belgarde, 2007). Dextral offset along the San Andreas fault translated the basin—and all crust southwest of the San Andreas —to the northwest relative to North America during Pliocene-Pleistocene filling of the basin.

A major tectonic reorganization at ca. 1.1–1.3 Ma terminated slip on the West Salton detachment fault along most of its length and initiated the modern San Jacinto, San Felipe, and Elsinore strike-slip faults (Figs. 1 and 2; Matti and Morton, 1993; Kirby, 2005; Lutz, 2005; Lutz et al., 2006; Steely, 2006; Kirby et al., 2007; Steely et al., 2009; Janecke et al., 2010). This event initiated present-day uplift and erosion of the southwestern parts of the former supradetachment basin in the western Salton Tough. The end of deposition and onset of uplift in the Fish Creek–Vallecito basin was part of this reorganization, and was related to initiation of currently active strike-slip faults at ca. 1 Ma (Johnson et al., 1983; Magistrale and Rockwell, 1996).

Fish Creek–Vallecito Basin

Sedimentary rocks of the Fish Creek–Vallecito basin are exposed in a thick SW-dipping section that ranges in age from Miocene to early Pleistocene (Figs. 2 and 3; Woodard, 1963, 1974; Opdyke et al., 1977; Johnson et al., 1983; Winker, 1987; Dibblee, 1996; Winker and Kidwell, 1996; Dorsey et al., 2007). Johnson et al. (1983) constructed a subsidence curve for this section using map-based estimates of present-day thicknesses and ages determined from paleomagnetic study. They implied that the base of the Imperial Formation is 4.3 Ma, but the base of their dated section is in the Mud Hills member of the Deguynos Formation, well above the base of the Imperial Group. Johnson et al. (1983) concluded that the basin underwent a gradual exponential decrease in subsidence rate, from 5.5 mm/yr to <0.5 mm/yr during the period 4.3–0.9 Ma. They attributed basin subsidence to continental rifting and crustal thinning and, by comparison to ocean basins, implied a thermal control on the exponential form of the subsidence curve.

Building on prior work of Woodard (1963), Winker and Kidwell (1996) elevated the formations of the Fish Creek–Vallecito basin to three groups: (1) the Miocene, nonmarine Split Mountain Group; (2) Lower Pliocene, marine Imperial Group; and (3) Pliocene-Pleistocene, nonmarine Palm Spring Group (Fig. 4). The oldest deposits predate strong extension and include nonmarine sandstone of the Red Rock Formation (exposed in Red Rock Canyon; Fig. 2) and overlying basaltic andesite of the 22–14 Ma Alverson volcanics (Ruisaard, 1979; Kerr, 1982; Winker and Kidwell, 1996). The base of the Elephant Trees Formation, and thus the onset of structurally controlled basin formation at Split Mountain Gorge, was dated at ca. 8.1 ± 0.4 Ma by Dorsey et al. (2007). This revised previous age estimates for the lower sandstone member of the Elephant Trees Formation, which had been correlated to the much older Red Rock Formation (Anza Formation of Woodard, 1963) in the western Fish Creek Mountains (Kerr, 1982; Kerr and Kidwell, 1991; Winker, 1987; Winker and Kidwell, 1996).

The Fish Creek–Vallecito basin is bounded on its NW and SW margin by the curviplanar, low-angle West Salton detachment fault, and on the SW by the strike-slip Elsinore fault zone (Fig. 2; Axen and Fletcher, 1998). In addition to Pliocene-Pleistocene slip on the detachment fault, the basin margin was active in middle to late Quaternary time, based on the presence of NW- and NE-trending fault scarps and faulted alluvial fans at the steep range front of the Tierra Blanca Mountains and around Whale Peak (Pinault, 1984; Magistrale and Rockwell, 1996; Todd, 2004; Kairouz, 2005). The faulted range front of the Tierra Blanca Mountains contains older strands of the detachment that are crosscut by younger strands of the active Elsinore fault zone (Dorsey and Axen, 2009).

METHODS

Geologic and Structural Mapping

We carried out detailed geologic and structural field mapping at scales of 1:10,000 to 1:24,000, integrated with analysis of air photos and high-resolution satellite imagery, to locate stratigraphic contacts and document major structures that must be identified in order to accurately reconstruct the section. Mapping and fault analysis are especially important in areas of structural complexity, where faults may offset the section and duplicate or cut out stratigraphic intervals. Through this work, we have identified the major structures that cross the section, thus providing a high degree of confidence in the thicknesses and ages of the section.

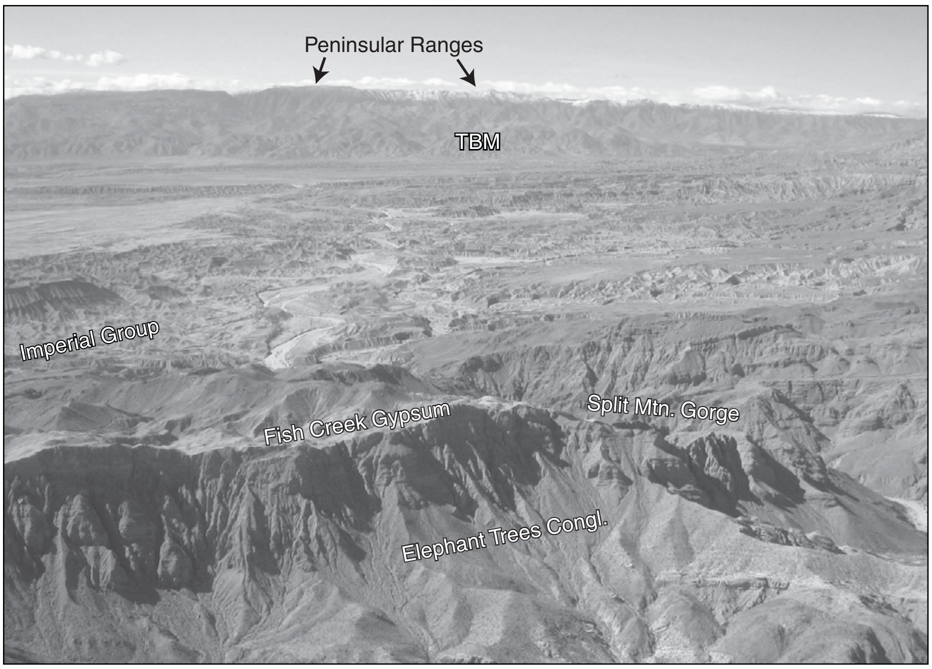

Figure 3. Oblique aerial photo looking southwest across the Fish Creek–Vallecito basin from above Split Mountain Gorge. Large low area in middle ground contains sediments dipping southwest away from viewer, and high topography in background is the eastern Peninsular Ranges and Tierra Blanca Mountains. See Figure 2 for location. TBM—Tierra Blanca Mountains.

Stratigraphic Thickness Data

Stratigraphic thicknesses were obtained for this study in two ways: (1) the lower 1240 m and the interval from 4450 to 5140 m (Fig. 5) were measured in the field using a Jacob's staff (data for the lower 1240 m modified slightly from Dorsey et al., 2007); and (2) thicknesses for the rest of the section were calculated from strike and dip of bedding at each paleomagnetic site augmented by strikes and dips at critical intervening locations, the location of each measurement within a strip map surrounding the transect, and a simple geometric model. The geometric model calculates stratigraphic thickness between stations using the sine of bedding dip, across-strike map distance, and changes in elevation (Compton, 1985). We tested this method by recalculating the thickness of segments that were measured by hand, and found that in most segments, the thickness calculated using the geometric model was within 2%–5% of that measured by hand. Stratigraphic thicknesses generated with this method are thus assigned a high level of confidence because bedding attitude is uniform over large areas, large structures are accounted for, bedding measurements are closely spaced (typically 30–100 m), and precise along-strike correlations were carried out using high-resolution air photos and satellite imagery.

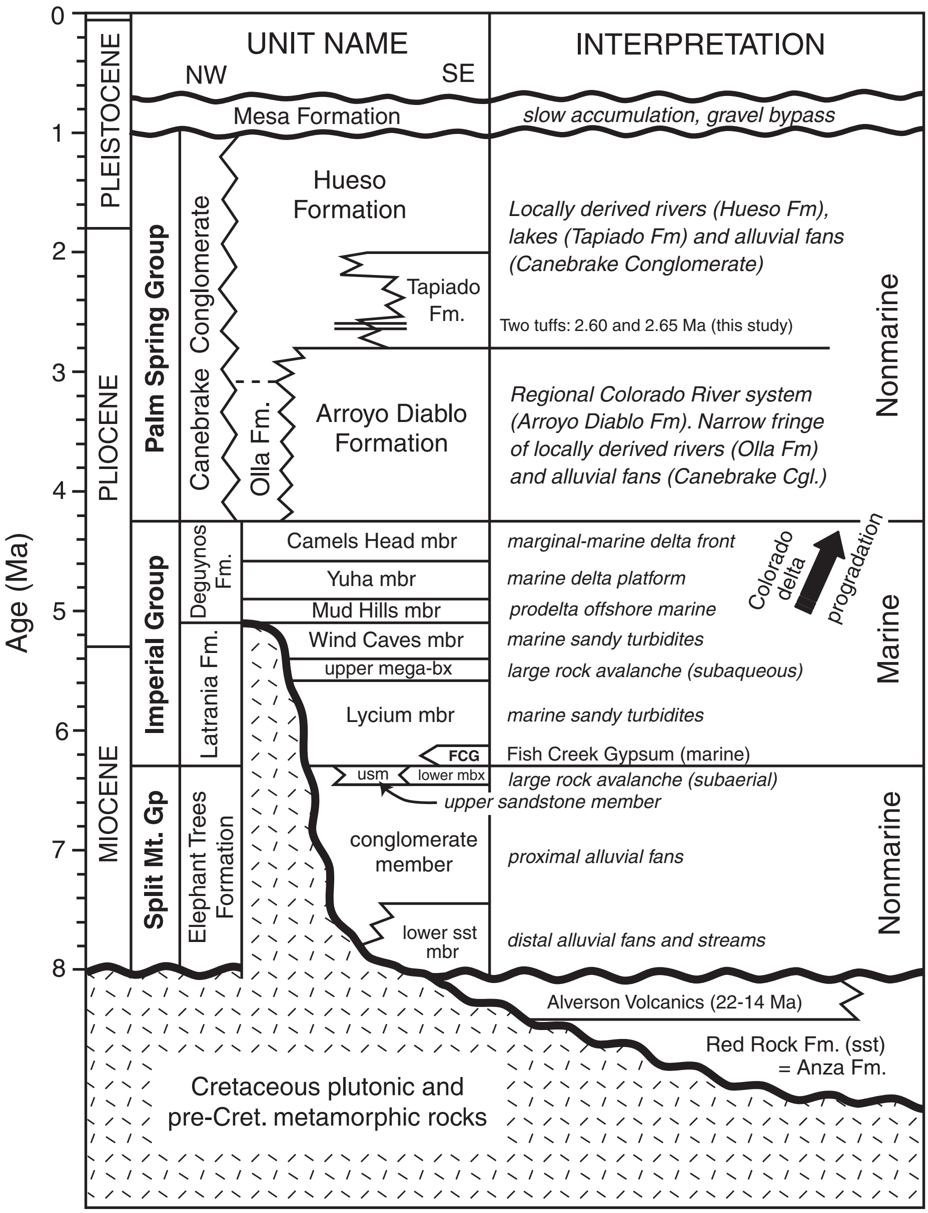

Figure 4. Chronostratigraphic diagram of sedimentary rocks in the Fish Creek–Vallecito basin. Stratigraphic nomenclature and interpretations are from Winker and Kidwell (1996), as modified slightly by Cassiliano (1999). Contact ages were determined or refined in this study. The base of the Elephant Trees Formation marks the earliest deposition related to onset of local deformation (extension or transtension) at ca. 8.0 ± 0.4 Ma (Dorsey et al., 2007). FCG—Fish Creek Gypsum; mbx—megabreccia.

Paleomagnetic Data

For this study, paleomagnetic samples were collected using either a portable drill, or as oriented block samples. Three to ten samples were collected at each site. Site locations were selected to maximize use of the existing ~130 sites collected and published by Opdyke et al. (1977) and Johnson et al. (1983). Notes and compilations of paleomagnetic results graciously provided by Everett Lindsay allowed us to locate the Opdyke/Johnson sample sites on our map, and thus to place their data accurately within the stratigraphic section (Fig. 5; see also GSA Data Repository items[1]). New sample sites were spaced stratigraphically closely together (10–30 m) in the Split Mountain Gorge area (Dorsey et al., 2007), and in portions of the upper 1500 km of the section, where previous data were lacking or where additional detail was needed to locate certain polarity boundaries. In other areas, wider (>100 m) spacing was employed to serve as validation and augmentation of existing data. In total, 77 new polarity determinations constrain the age of the measured section along dry washes in the study area (Figs. 2 and 5).

Paleomagnetic samples were cut into standard-sized specimens and measured in the Western Washington University paleomagnetism laboratory using a 2-G 755-R Cryogenic magnetometer. Specimens were subjected to stepwise thermal or alternating field demagnetization (or in some cases both). Orthogonal vector plots and stereographic projections were used to determine the characteristic magnetization and magnetic polarity of the specimens,

[1]GSA Data Repository item 2010211, Table DR1 (GPS locations, thicknesses, polarity determinations, and data quality for all paleomagnetic samples), Table DR2 (locations of Opdyke et al. [1977] sites, and comparison of their results with results of this study), Figure DR1 (expanded stratigraphic column showing position and number of paleomagnetic sampling sites), are available online at www.geosociety.org/pubs/ft2010.htm, or on request from editing@geosociety.org or Documents Secretary, GSA, P.O. Box 9140, Boulder, CO 80301, USA.

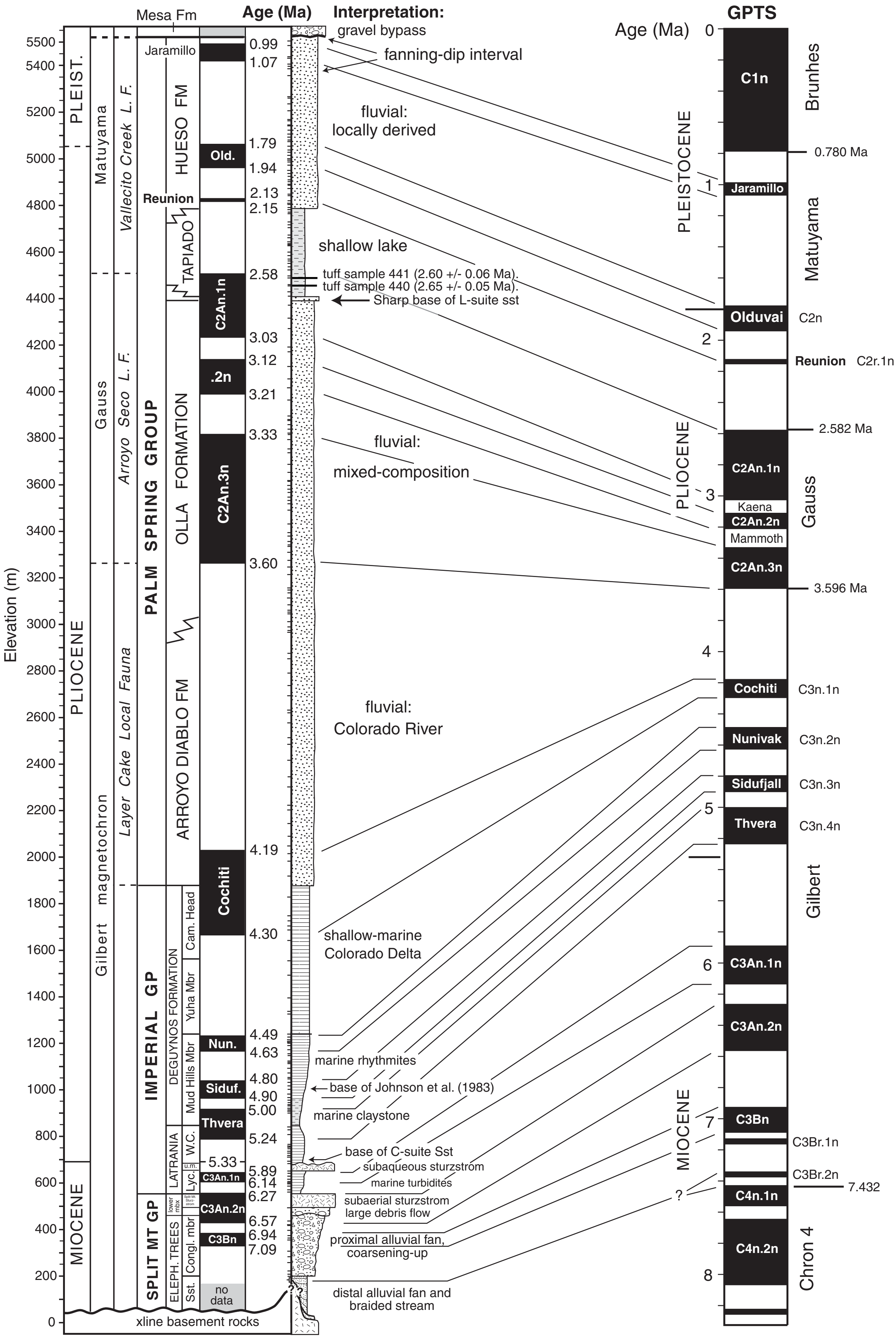
Mesa Fm
Age (Ma)
Interpretation:
gravel bypass
fanning-dip interval
fluvial: locally derived
shallow lake
tuff sample 441 (2.60 +/- 0.06 Ma).
tuff sample 440 (2.65 +/- 0.05 Ma).
Sharp base of L-suite sst
fluvial: mixed-composition
fluvial: Colorado River
shallow-marine Colorado Delta
marine rhythmites
base of Johnson et al. (1983)
marine claystone
base of C-suite Sst
subaqueous sturzstrom
marine turbidites
subaerial sturzstrom large debris flow
proximal alluvial fan, coarsening-up
distal alluvial fan and braided stream
Elevation (m)
PLEIST.
PLIOCENE
MIOCENE
Matuyama
Gauss
Gilbert magnetochron
Vallecito Creek L. F.
Arroyo Seco L. F.
Layer Cake Local Fauna
PALM SPRING GROUP
IMPERIAL GP
SPLIT MT GP
HUESO FM
TAPIADO
OLLA FORMATION
ARROYO DIABLO FM
DEGUYNOS FORMATION
LATRANIA
ELEPH. TREES
Cam. Head
Yuha Mbr
Mud Hills Mbr
W.C.
Lyc.
Congl. mbr
Sst.
Jaramillo
Old.
Reunion
C2An.1n
.2n
C2An.3n
Cochiti
Nun.
Siduf.
Thvera
C3An.1n
C3An.2n
C3Bn
no data
xline basement rocks
0.99
1.07
1.79
1.94
2.13
2.15
2.58
3.03
3.12
3.21
3.33
3.60
4.19
4.30
4.49
4.63
4.80
4.90
5.00
5.24
5.33
5.89
6.14
6.27
6.57
6.94
7.09
GPTS
Age (Ma)
Brunhes
C1n
0.780 Ma
Jaramillo
PLEISTOCENE
Matuyama
Olduvai C2n
Reunion C2r.1n
2.582 Ma
C2An.1n
Kaena
C2An.2n
Mammoth
C2An.3n
PLIOCENE
Gauss
3.596 Ma
Cochiti C3n.1n
Nunivak C3n.2n
Sidufjall C3n.3n
Thvera C3n.4n
Gilbert
C3An.1n
C3An.2n
C3Bn
C3Br.1n
C3Br.2n
7.432
C4n.1n
C4n.2n
MIOCENE
Chron 4

Figure 5. Composite section for the Fish Creek–Vallecito basin showing thicknesses, stratigraphic position of paleomagnetic sample sites, and correlation of reversals to the geomagnetic polarity time scale (GPTS). Tick marks left of lithic log indicate position of samples collected for paleomagnetic study (see Fig. DR1 and Table DR1 [see text footnote 1]). Stratigraphic nomenclature is from Winker and Kidwell (1996), as modified slightly by Cassiliano (1999).

along with a qualitative assessment of the quality of the polarity determination for each site.

U-Pb Zircon Methods

Zircon grains were separated from total rock samples using standard crushing, washing, heavy-liquid (specific gravity 2.96 and 3.3), and paramagnetic procedures. Hand-selected zircon grains were placed onto double-sided tape, mounted in epoxy together with grains of the Temora reference zircon, sectioned approximately in half, and polished. Reflected and transmitted light photomicrographs were prepared for all zircons, as were cathodoluminescence (CL) scanning electron microscope (SEM) images. The CL images were used to decipher the internal structures of the sectioned grains and to ensure that the ~20 μm sensitive high-resolution ion microprobe (SHRIMP) spot was wholly within a single age component in the sectioned grains.

The U-Th-Pb analyses were made using SHRIMP IIe at Geoscience Australia, Canberra, Australia, following procedures given in Williams (1998, and references therein). Each analysis consisted of six scans through the mass range, with the Temora reference zircon grains analyzed after every three unknown analyses. The data were reduced using the SQUID Excel macro of Ludwig (2001). The Pb/U ratios were normalized relative to a value of 0.0668 for the FC1 reference zircon, equivalent to an age of 417 Ma (see Black et al., 2003). Uncertainty in the Temora U/Pb ratio calibration was 0.39% for the SHRIMP IIe session. Due to the young age of the zircon grains, the U-Pb data need to be corrected for ^{230}Th disequilibrium that induces a deficit of ^{206}Pb in Th-poor minerals such as zircon (Schärer, 1984). This was done using the ^{232}Th/^{238}U measured ratio in the zircon and assuming a Th/U ratio of the magma in equilibrium with the crystallizing zircon. We used a Th/U ratio of 2.25 for the magma based on whole-rock geochemical data in Sarna-Wojcicki et al. (2005) for tuffs that likely have the same source (Long Valley caldera, eastern California) as the two tuffs analyzed in this study. This is similar to the value of 2.2 that was used by Schmitz and Bowring (2001) for the Fish Canyon Tuff.

Uncertainties given for individual analyses (ratios and ages) are at the 1σ level (Table 1). Tera and Wasserburg (1972) concordia plots, probability density plots with stacked histograms, and

TABLE 1. U-Pb ZIRCON SENSITIVE HIGH-RESOLUTION ION MICROPROBE (SHRIMP) DATA

							Total corrected for ^{230}Th disequilibrium					Radiogenic		Age (Ma)	
Grain spot	U (ppm)	Th (ppm)	Th/U	^{206}Pb* (ppm)	^{204}Pb/^{206}Pb	f_{206} %	^{238}U/^{206}Pb	±	^{207}Pb/^{206}Pb	±	f Th/U	^{206}Pb/^{238}U	±	^{206}Pb/^{238}U	±
TAL 6071															
1.1	476	344	0.72	0.17	0.012913	4.36	2352	74	0.0805	0.0144	0.321	0.00041	0.00001	2.62	0.09
2.1	716	696	0.97	0.27	0.000320	3.38	2262	54	0.0728	0.0075	0.432	0.00043	0.00001	2.75	0.07
3.1	409	295	0.72	0.15	0.001510	4.15	2287	76	0.0789	0.0118	0.320	0.00042	0.00001	2.70	0.09
4.1	579	477	0.82	0.30	0.013868	33.77	1646	45	0.3128	0.0493	0.366	0.00040	0.00004	2.59	0.25
5.1	536	320	0.60	0.19	0.003964	5.37	2374	65	0.0885	0.0094	0.266	0.00040	0.00001	2.57	0.07
6.1	510	337	0.66	0.20	–	3.39	2121	61	0.0728	0.0094	0.293	0.00046	0.00001	2.94	0.09
7.1	412	269	0.65	0.15	0.012453	11.42	2283	66	0.1363	0.0122	0.291	0.00039	0.00001	2.50	0.08
8.1	694	559	0.81	0.26	0.004136	5.47	2270	53	0.0893	0.0075	0.358	0.00042	0.00001	2.68	0.06
9.1	292	163	0.56	0.11	0.022144	11.39	2135	78	0.1360	0.0156	0.248	0.00041	0.00002	2.67	0.11
10.1	866	739	0.85	0.32	0.006320	6.46	2279	53	0.0971	0.0069	0.379	0.00041	0.00001	2.64	0.06
11.1	558	399	0.71	0.21	0.018499	6.00	2276	66	0.0935	0.0094	0.317	0.00041	0.00001	2.66	0.08
12.1	616	473	0.77	0.31	0.024015	30.05	1662	36	0.2834	0.0123	0.342	0.00042	0.00001	2.71	0.08
13.1	665	475	0.71	0.25	0.002934	9.03	2245	59	0.1174	0.0094	0.317	0.00041	0.00001	2.61	0.07
14.1	419	313	0.75	0.15	0.003105	8.54	2384	77	0.1135	0.0124	0.331	0.00038	0.00001	2.47	0.09
15.1	824	785	0.95	0.29	0.008376	5.45	2353	52	0.0891	0.0070	0.423	0.00040	0.00001	2.59	0.06
16.1	1280	1357	1.06	0.47	–	2.38	2269	45	0.0649	0.0047	0.471	0.00043	0.00001	2.77	0.05
17.1	387	240	0.62	0.14	0.010573	10.81	2249	69	0.1314	0.0125	0.276	0.00040	0.00001	2.55	0.09
18.1	529	530	1.00	0.20	0.004746	7.79	2218	58	0.1076	0.0094	0.445	0.00042	0.00001	2.68	0.08
TAL 6073															
2.1	840	867	1.03	0.31	0.006094	5.54	2282	51	0.0898	0.0069	0.459	0.00041	0.00001	2.67	0.06
3.1	290	146	0.51	0.10	0.027209	15.22	2306	84	0.1662	0.0176	0.225	0.00037	0.00002	2.37	0.10
4.1	577	450	0.78	0.21	–	6.94	2287	65	0.1009	0.0096	0.346	0.00041	0.00001	2.62	0.08
5.1	285	236	0.83	0.10	–	9.95	2300	109	0.1247	0.0386	0.369	0.00039	0.00003	2.52	0.18
7.1	483	182	0.38	10.47	0.000058	0.18	39.63	0.44	0.0507	0.0008	0.167	0.02510	0.00028	160.3	1.8
8.1	395	269	0.68	0.14	0.013523	7.03	2353	79	0.1016	0.0115	0.303	0.00039	0.00001	2.55	0.09
9.1	256	160	0.62	0.10	0.031353	11.70	2226	88	0.1385	0.0160	0.277	0.00040	0.00002	2.56	0.11
10.1	476	143	0.30	6.20	0.000481	0.10	66.01	0.75	0.0487	0.0010	0.133	0.01511	0.00017	96.8	1.1
11.1	311	186	0.60	0.16	0.012386	23.87	1604	49	0.2346	0.0159	0.267	0.00047	0.00002	3.05	0.12
12.1	176	99	0.57	0.07	0.027240	17.60	2098	89	0.1850	0.0225	0.251	0.00039	0.00002	2.53	0.13
13.1	380	161	0.42	0.13	0.014739	8.24	2375	75	0.1112	0.0124	0.188	0.00039	0.00001	2.49	0.08
14.1	180	112	0.62	0.07	0.035050	14.79	2089	87	0.1629	0.0258	0.277	0.00041	0.00002	2.63	0.14
16.1	316	211	0.67	0.11	–	10.89	2384	90	0.1321	0.0159	0.297	0.00037	0.00002	2.41	0.10
17.1	222	141	0.64	0.09	–	10.77	2113	81	0.1311	0.0174	0.283	0.00042	0.00002	2.72	0.12
18.1	565	468	0.83	0.20	–	4.22	2357	62	0.0795	0.0087	0.368	0.00041	0.00001	2.62	0.07
19.1	415	283	0.68	0.17	–	3.05	2070	64	0.0702	0.0094	0.304	0.00047	0.00001	3.02	0.10
20.1	235	175	0.74	0.09	0.019862	10.85	2078	77	0.1318	0.0161	0.330	0.00043	0.00002	2.76	0.12

Note: (1) Uncertainties are given at the 1σ level. (2) Error in Temora reference zircon calibration was 0.39% for the analytical session (not included in above errors but required when comparing data from different mounts). (3) f_{206} % denotes the percentage of ^{206}Pb that is common Pb. (4) Correction for common Pb for the U/Pb data has been made using the measured ^{238}U/^{206}Pb and ^{207}Pb/^{206}Pb ratios following Tera and Wasserburg (1972) as outlined in Williams (1998). (5) f Th/U denotes the degree of Th-U fractionation between mineral and magma, which is given by $f = (Th/U)_{mineral}/(Th/U)_{magma}$. For this sample, we have assumed Th/U = 2.25 for the magma. (6) In the case of zircon, a correction for a deficit of ^{206}Pb is required, due to a deficiency of ^{230}Th (Schärer, 1984): $(\lambda_{238}/\lambda_{230})$ (f – 1).

weighted mean $^{206}Pb/^{238}U$ age calculations were generated using ISOPLOT/EX (Ludwig, 2003). Weighted mean $^{206}Pb/^{238}U$ ages were calculated, and the uncertainties are reported as 95% confidence limits. The decay constants used are those recommended by the International Union of Geological Sciences (IUGS) Subcommission on Geochronology (Steiger and Jäger, 1977).

Decompaction and Backstripping

Accurate reconstruction of long-term basin subsidence requires use of numerical methods that correct for loss of pore space during progressive burial and compaction of sediment. We used the method of Angevine et al. (1990), which is adapted from previous studies (Van Hinte, 1978; Sclater and Christie, 1980; Bond et al., 1983). This approach assumes that porosity varies as a function of depth and lithology, and that pore spaces are interconnected (i.e., no overpressured zones). The decompaction algorithm employs empirically derived, lithology-dependent, porosity-depth relationships that follow an exponential decrease in porosity with depth (e.g., Sclater and Christie, 1980; Bond et al., 1983). The section was decompacted by calculating the effects of removing successively older units from the top and allowing the section to expand as underlying units are unloaded. Tectonic subsidence is defined as the component of total subsidence attributed to a tectonic driving force, and is calculated by removing the effect of the sediment load assuming a local (Airy) isostatic response to sediment loading.

For the subsidence analysis, we assumed that stratigraphic thickness—corrected for the effects of compaction and sea level—represents the total depth of the basin through time. Alternatively, if the section was progressively tilted above the West Salton detachment fault during deposition, the total depth of the basin would be less than the measured stratigraphic thickness. We rule out this possibility based on the overall uniform bedding dips through all but the upper ~150 m of the section, which indicate that tilting took place after deposition. The analysis also assumes that nonmarine sediments were accumulated close to sea level, as indicated by the present-day distribution of fluvial environments in the modern Salton Trough (Fig. 1).

Possible Sources of Error

Faults

Offset on faults can juxtapose different parts of an original stratigraphic section and, if offset strata are incorrectly correlated, can produce error in measurements of stratigraphic thickness. Large unrecognized fault offsets may also result in omission or duplication of magnetic reversals. Through detailed geologic and structural mapping, we have identified and quantified most or all of the large fault offsets in the studied section. Some uncertainty persists in one area where the section crosses the upper Wind Caves and lower Mud Hills Members (Fig. 2), which are cut by a series of incompletely mapped right-lateral and left-lateral strike-slip faults. Some of these faults are potentially large and have latest Quaternary fault scarps, yet were not observed along strike in the measured section. This introduces potential error to the thickness of the upper Wind Caves and lower Mud Hills Members (likely ≤30–50 m), which likely does not alter the main conclusions of this study.

Ages of Magnetic Reversals

Ages in this section are based on correlation of the observed paleomagnetic reversals to the global geomagnetic polarity time scale (GPTS; Cande and Kent, 1995; Lourens et al., 1996; Gradstein et al., 2004). Correct correlation to the GPTS requires independent age controls such as isotopically dated tuffs or biostratigraphic markers, both of which are present in the Fish Creek–Vallecito basin. Even with independent age controls, correlation to the GPTS can be incorrect if unconformities are present but not recognized, if parts of the section are duplicated or omitted by unmapped faults, or if magnetic polarities are misidentified due to incompletely removed modern magnetic overprint.

Thickness and Emplacement of Megabreccias

The two megabreccias in the upper Split Mountain Group and lower Imperial Group display considerable lateral variations in thickness, which can potentially affect the shape of the subsidence curve. Because previous studies have shown that the megabreccias were emplaced instantaneously (e.g., Kerr and Abbott, 1996; Winker and Kidwell, 1996; Abbott et al., 2002), we assume that they represent little or no time. In both subaerial and subaqueous environments, it is likely that a short-lived hiatus formed on the upper surface of a megabreccia during the time it took for background deposition to accumulate sediment up to that surface. We thus assume that the thickness of a megabreccia represents an amount of time similar to an equivalent thickness of background sediment. This is a simplifying assumption that does not account for possible erosion or soft-sediment deformation during emplacement of the megabreccia, or other related complicating factors.

Estimates of Paleobathymetry

The shape of any subsidence curve that includes marine deposits is dependent on estimates of water depth, which typically are based on fossils preserved in the section (e.g., Van Hinte, 1978; Angevine et al., 1990). Paleo–water depths must be bracketed within a range of possible end members, and the subsidence curve is then bracketed using this range. Estimates of paleo–water depth in the marine part of the section are subject to large uncertainties because of two plausible interpretations (minimum and maximum water depth) of micropaleontology data presented by Dorsey et al. (2007).

Paleo-Elevation of Nonmarine Deposition

The geohistory analysis assumes that nonmarine deposits of the Split Mountain and Palm Spring Groups accumulated slightly above sea level. However, it is possible that the Split Mountain Group accumulated in an active basin either above or below sea level, and remained subaerial for a period of time due to the presence of topographic barriers. Based on comparison to the modern Salton Sea, which is ~70 m below sea level, we infer that this uncertainty may introduce ~50–100 m of uncertainty in the subsidence analysis prior to 6.3 Ma. Similarly, by comparison to elevations in the modern Salton Trough region, we assume that fluvial and deltaic deposits of the Pliocene Palm Spring Group accumulated at or near sea level, thus introducing a similar error of ±50–100 m. This magnitude of error is small compared to the large thickness of the section, and therefore it does not significantly affect the overall shape of the subsidence curve.

RESULTS

Lithostratigraphy

The total thickness of the section is slightly over 5500 m from the base of the Elephant Trees Formation to the unconformable top of the Hueso Formation (Fig. 5; Fig. DR1 [see footnote 1]). We use the stratigraphic nomenclature of Winker and Kidwell (1996), as modified slightly by Cassiliano (1999), in which the Split Mountain, Imperial, and Palm Spring Formations are elevated to group status, and some members of Winker (1987) are elevated to formation status.

Split Mountain and Imperial Groups

The lower sandstone member of the Elephant Trees Formation is exposed east of Split Mountain Gorge (Fig. 2) in a small paleovalley, where it rests on Cretaceous tonalite and is conformably overlain by coarse bouldery conglomerate (Figs. 5 and 6A). There, the lower sandstone member is estimated to be 150–200 m thick based on detailed geologic mapping, eye-height measurements, and visual inspection (Shirvell, 2006; Dorsey et al., 2007; this study). Elsewhere, the lower sandstone member is thin to absent, onlaps a buttress unconformity, and passes laterally into conglomerate that also rests directly on pre-Cenozoic crystalline rocks (Shirvell, 2006). Red sandstone exposed beneath conglomerate on the west side of the main wash in Split Mountain Gorge reveals a progressive unconformity (angular unconformity that passes laterally into a concordant contact), and records local tilting to the southeast during deposition of the upper part of the lower sandstone member. Thick alluvial-fan conglomerate of the Elephant Trees Formation is capped by the lower megabreccia landslide derived from the nearby Vallecito Mountains (Figs. 5 and 6B; Winker and Kidwell, 1996; Abbott et al., 2002; Shirvell, 2006).

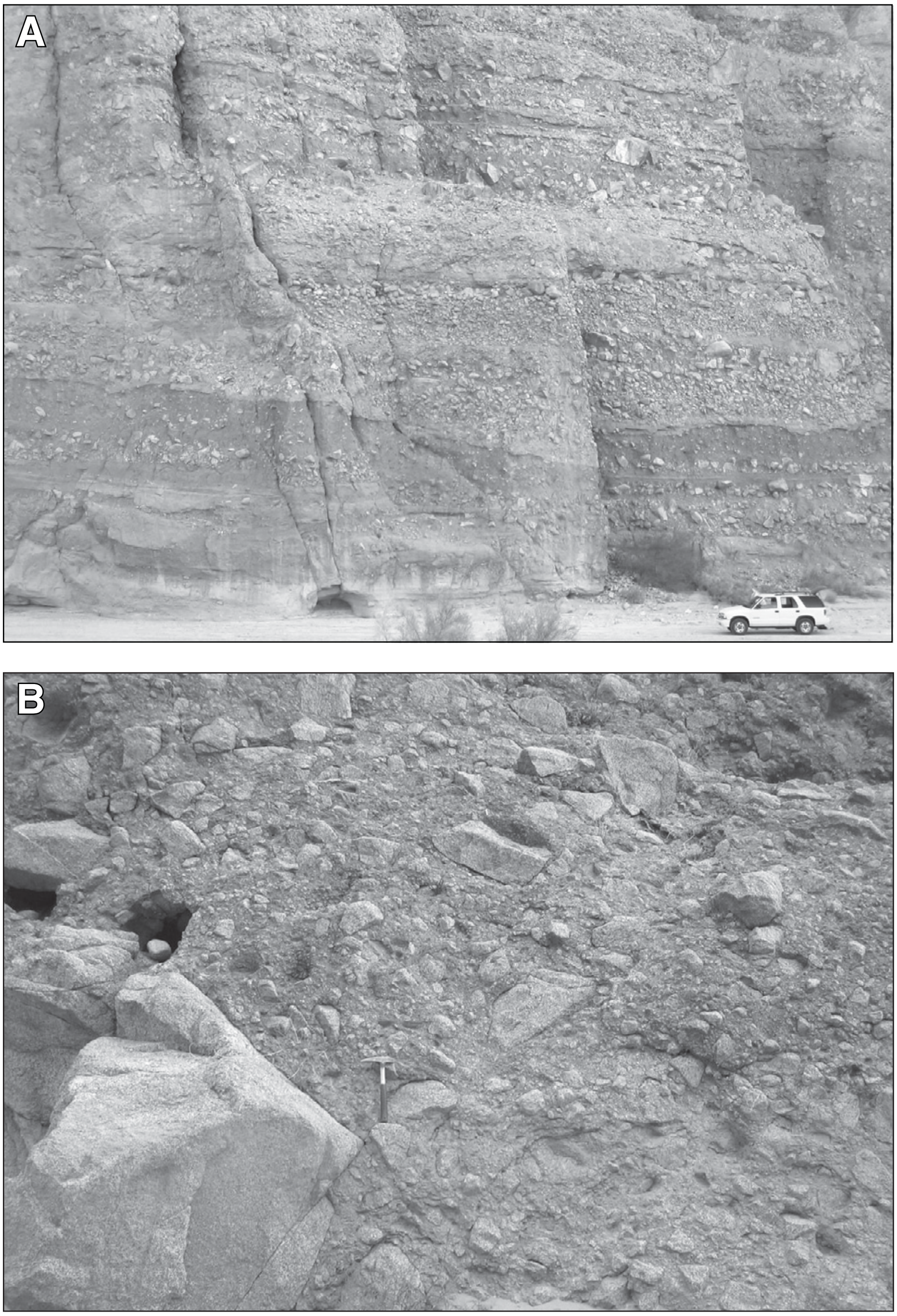

Figure 6. Field photos of the Split Mountain Group in the lower part of the section. (A) Coarse bouldery conglomerate of the Elephant Trees Formation records deposition by debris flows and sheet floods in a fault-bounded alluvial fan. (B) Detail of the lower megabreccia.

The lower megabreccia is overlain along a sharp irregular surface by marine mudstone and locally derived turbidites at the base of the marine Imperial Group (Fig. 7). The oldest marine deposits interfinger laterally with the Fish Creek Gypsum and are dated at ca. 6.3 Ma with magnetostratigraphy (Fig. 5). About 2 km north of the measured section, the base of the Imperial Group is marked by an ~50–70-m-thick conformable transition from nonmarine conglomerate of the Elephant Trees Formation through subaqueous conglomerate and sandy turbidites into marine mudstone of the lower Latrania Formation, and the lower megabreccia is absent. This and other rapid lateral facies changes in the Split Mountain area provide evidence for steep paleoslopes and complex local paleogeography that were controlled by active extensional or transtensional structures prior to and during latest Miocene marine incursion (e.g., Winker and Kidwell, 1996; Shirvell, 2006). The observed correlation to a conformable transition indicates that very little time is missing across the contact between the lower megabreccia and marine Latrania Formation in the measured section (Fig. 5).

The earliest input of sediment from the Colorado River is based on first appearance of fine-grained, well-rounded quartz sand with distinctive hematite coatings in sandy turbidites of the lower Wind Caves Member at 702 m in the section, 140 m above the base of marine deposits (Fig. 5; Gastil et al., 1996; Winker and Kidwell, 1996; Dorsey et al., 2007). Above that, sandy turbidites display gradual fining-up into ~100 m of marine mudstone and claystone in the lower Mud Hills Member of the Deguynos Formation (Fig. 5). The claystone is a regionally extensive marine unit also known as "Coyote Clays" (Hanna, 1926; Jefferson and Lindsay, 2006) that records a short-lived reduction of sand-sized clastic input to the basin. It is in turn gradationally overlain by marine rhythmites of the upper Mud Hills Member (Figs. 5 and 8C; Winker, 1987). The rhythmites are overlain by fossiliferous sandstone and mudstone of the Yuha and Camels Head Members of the Deguynos Formation, which were deposited in the shallow-marine part of the prograding Colorado River delta (Winker, 1987; Winker and Kidwell, 1996). The top of the Deguynos Formation is a well-defined conformable transition to fluvial deposits of the Arroyo Diablo Formation (Fig. 5).

Palm Spring Group

The Palm Spring Group is subdivided into two main intervals (Figs. 4 and 5). The lower interval consists of laterally equivalent facies of the Arroyo Diablo and Olla Formations and Canebrake Conglomerate. The Arroyo Diablo Formation contains well-sorted, fine-grained, quartz-rich sandstone and mudstone that accumulated in the nonmarine portion of the Colorado River delta (Fig. 8D; Winker, 1987; Winker and Kidwell, 1996). Paleocurrent measurements reveal significant scatter, with overall transport to the south (Winker and Kidwell, 1986). Winker and Kidwell (1986) interpreted this to record original transport to the southeast after correcting for ~35° of postdepositional clockwise rotation (Johnson et al., 1983). Recent paleomagnetic studies suggest ~24° of clockwise rotation between ca. 4.0 and 2.5 Ma, during deposition of the Arroyo Diablo Formation (Housen et al., 2005, 2006). The implied syndepositional rotation history suggests a need for reconstruction of paleocurrents at a level of detail that is not possible with the available data. We therefore infer that fluvial transport was generally toward the south to SSE during deposition of the Arroyo Diablo Formation between 4.2 and 2.8 Ma.

The Arroyo Diablo Formation passes laterally to the northwest into the Olla Formation, a fluvial unit that contains more than ~20%–50% distinctive interbeds of arkosic and detrital mica-rich locally derived sandstone and passes laterally northward into the Canebrake Conglomerate (Fig. 2; Winker, 1987; Winker and Kidwell, 1996; Kairouz, 2005). The Canebrake Conglomerate is age-equivalent to both the lower and upper intervals of the Palm Spring Group (Fig. 4), and it consists of pebble- to cobble-boulder conglomerate that accumulated in alluvial fans around the fault-bounded margins of the basin. North of the Vallecito Mountains, Canebrake Conglomerate in the lower Palm Spring interval is faulted against the West Salton detachment fault (Steely et al., 2009; Belgarde, 2007; Matti et al., 2002).

The upper interval of the Palm Spring Group consists of the Hueso and Tapiado Formations and laterally equivalent Canebrake Conglomerate (Figs. 4 and 5). The contact with underlying deposits is sharp but conformable, and, where it overlies the Arroyo Diablo Formation, the contact is marked by an abrupt change from Colorado River–derived to locally derived sand composition (Winker, 1987; this study). The Tapiado Formation consists of interbedded lacustrine mudstone, siltstone, and sandstone that passes laterally to the northwest and southeast into the lower part of the Hueso Formation (Figs. 2 and 8E; Winker, 1987). Two fine-grained air-fall tuffs provide critical age control in the lower 100 m of the Tapiado Formation (Fig. 5; Fig. DR1 [see footnote 1]). The Hueso Formation contains locally derived fluvial sandstone, conglomerate, and thin-bedded sandstone with mudstone transitional to the Tapiado Formation (Fig. 8F). The upper interval of the Canebrake Conglomerate rests in fault contact on the low-angle West Salton detachment fault, thus defining the steep proximal margin of the Pliocene-Pleistocene supradetachment basin (Axen and Fletcher, 1998; Kairouz, 2005).

The contact between the Hueso Formation and overlying Quaternary gravel (Mesa Formation of Woodard, 1963) is marked by an ~150–200-m-thick interval of fanning dips that begins slightly below the base of the Jaramillo subchron (1.07 Ma) and contains reworked sandstone clasts, paleosols, and restricted lacustrine deposits (Fig. 5). This fanning-dip interval records the onset of tilting at ca. 1.1–1.2 Ma (Dorsey and Axen, 2009). The base of the Mesa Formation is ~30 m above the top of the Jaramillo subchron and is estimated to be ca. 0.95 Ma.

Tuff Ages

Sample 02–440 (4454 m above Base of Section)

About 50 zircon grains were handpicked from the heavy mineral concentrate of sample 02–440. The zircon grains are euhedral, equant to elongate crystals with bipyramidal terminations, or they are fragments of such grains. They are ≤100 μm in length. The CL images show a simple oscillatory-zoned internal structure, with some grains having broad even CL zonation. For this study, 18 grains were analyzed because many of the zircons were cracked or irregular fragments and not ideal even for the 20-μm-diameter SHRIMP spot diameter (Table 1). Two of the areas analyzed were significantly enriched in common Pb, with measured total $^{207}Pb/^{206}Pb$ ratios of ~0.3. The other 16 analyses were more enriched in radiogenic Pb, but the $^{207}Pb/^{206}Pb$ ratios were elevated, in the range ~0.065 to ~0.136. The calculated radiogenic $^{206}Pb/^{238}U$ ages show a simple bell-shaped distribution on a relative probability plot (Fig. 9A). If the slightly older analysis of grain 6

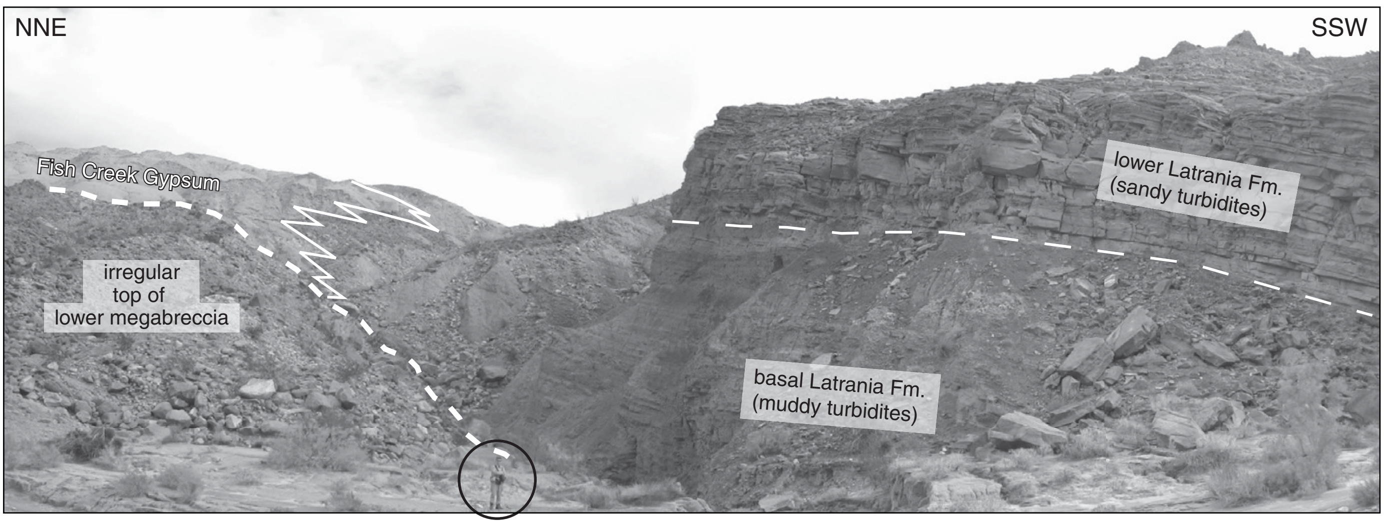

Figure 7. Field photo looking approximately ESE at the irregular top of the lower megabreccia (emplaced in a subaerial alluvial-fan setting), and directly overlying marine turbidites of the basal Latrania Formation and laterally equivalent Fish Creek Gypsum in the lowermost Imperial Group. Person standing in foreground (circled) for scale. The basal contact of the Imperial Group records rapid marine incursion at ca. 6.3 Ma.

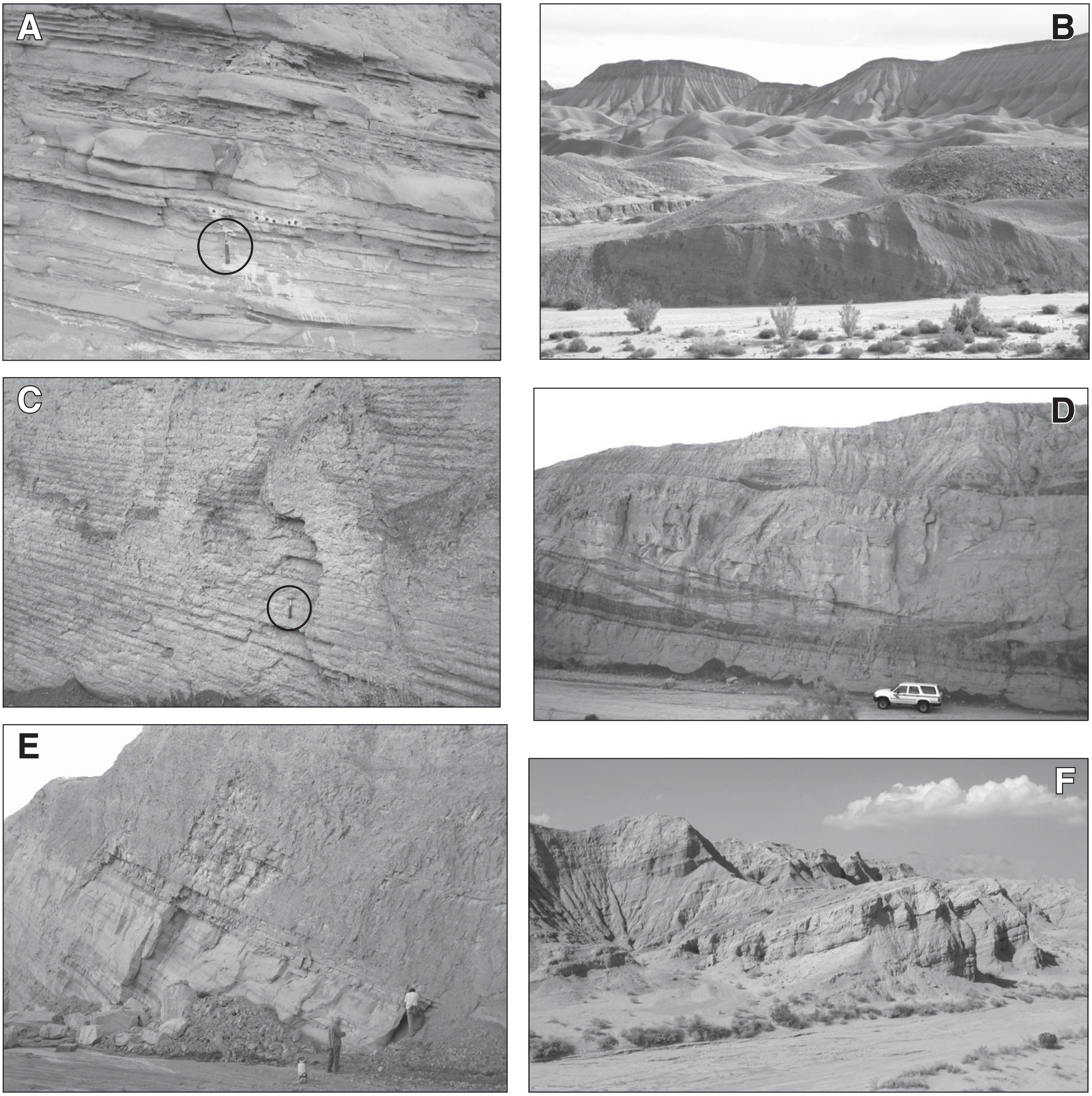

Figure 8. (A) Sandy turbidites of the Latrania Formation, showing a typical paleomagnetic sampling site (~590 m in section; Fig. 5). Hammer (circled) is 32.5 cm long. (B) Transition from muddy turbidites of the upper Latrania Formation (foreground) to marine claystone in the lower Mud Hills Member of the Deguynos Formation (middle ground). Ridge in distance is held up by shallow-marine calcarenite and shell beds at the base of the Yuha Member of the Deguynos Formation (Fig. 5). View shows about 400 meters of section. (C) Marine rhythmites of the Mud Hills Member (~1070 m in Fig. 5). Hammer (circled) is 32.5 cm long. (D) Channelized, cross-bedded sandstone and interbedded mudstone of the Arroyo Diablo Formation (Palm Spring Group). (E) Tabular-bedded lacustrine mudstone and sandstone of the Tapiado Formation. (F) Interbedded fluvial sandstone and mudstone of the Hueso Formation. Resistant sandstone unit in right center of photo is 5.5 m thick.

($^{206}Pb/^{238}U$ age of ca. 2.94 Ma) is excluded, the weighted mean age is 2.65 ± 0.05 Ma (mean square of weighted deviates [MSWD] = 1.3; uncertainty given as 95% confidence limits). This is interpreted as recording the time of zoned igneous zircon crystallization.

Sample 02–441 (4488 m above Base of Section)

Slightly more zircon grains (~65) were hand selected from the heavy mineral concentrate of sample 02–441. The zircon grains have a wider size range, up to 200 µm in length, with most being ≤100 µm. The morphology is also more variable. Euhedral, elongate to equant crystals with pyramidal terminations are the more dominant; however, equant to elongate round grains are also present and clearly have undergone considerable surface transport. These were interpreted to be reworked detrital grains and are quite distinct from the euhedral, igneous zircon. For the fresh igneous zircons, the CL images once again show a simple oscillatory-zoned internal structure with some sector zoning.

For this study, 17 grains were analyzed, as once again, many of the zircons were cracked or irregular fragments, or were clearly detrital (Table 1). Two of the grains analyzed are significantly older, with $^{206}Pb/^{238}U$ ages of ca. 160 Ma (grain 7) and ca. 97 Ma (grain 10). These are not shown on the relative probability plot (Fig. 9B), nor are they considered further in this discussion. The analyses of grains 11 and 19 yield a $^{206}Pb/^{238}U$ age of ca. 3.0 Ma, similar to that for grain 6 in sample 02–440. These are interpreted as slightly older magmatic zircons that were incorporated into the ash deposit. The calculated radiogenic $^{206}Pb/^{238}U$ ages for the remaining 13 analyses show a relatively simple bell-shaped distribution on a relative probability plot (Fig. 9B), though the curve is skewed to the younger age side. If the slightly younger analysis of grain 3 ($^{206}Pb/^{238}U$ age of ca. 2.37 Ma) is excluded, the weighted mean age is 2.60 ± 0.06 Ma (MSWD = 0.97; uncertainty given as 95% confidence limits). As with sample 02–440, this is interpreted to record the time of zoned igneous zircon crystallization.

The source of the two dated tuffs is uncertain but may be the Long Valley caldera in eastern California, which experienced many late Pliocene to Pleistocene eruptions and repeatedly deposited ash layers around southern California and Nevada (e.g., Sarna-Wojcicki et al., 1984, 1997, 2005). The two tuffs in this section are 21 and 55 m beneath the Gauss-Matuyama reversal, similar to a group of tuffs named the "tuffs of the Badlands (lower set)" that are found in a 50 m interval below the Gauss-Matuyama boundary near Long Valley (Sarna-Wojcicki et al., 2005).

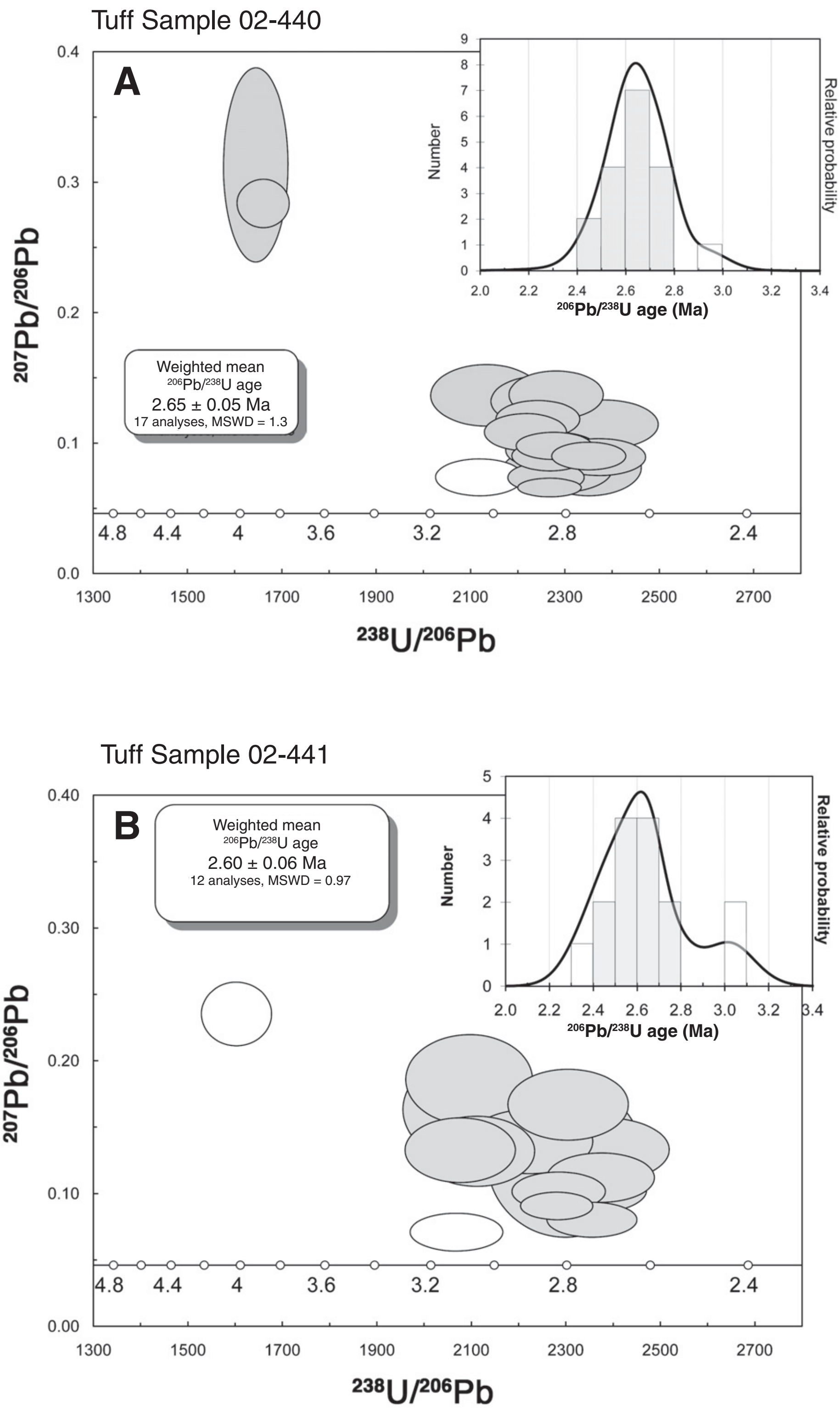

Figure 9. Tera-Wasserburg concordia plots of sensitive high-resolution ion microprobe (SHRIMP) U-Pb zircon data for tuffaceous rock samples 02–440 (A) and 02–441 (B). Data are plotted as 1σ error ellipses. Insets show the relative probability plots of the $^{206}Pb/^{238}U$ ages. Weighted mean age calculation results are also shown, with age uncertainties given as 95% confidence limits. MSWD—mean square of weighted deviates.

Based on their similar stratigraphic position, we speculate that these tuffs may have been produced by the same eruptions at Long Valley.

Magnetostratigraphy

The results of the demagnetization experiments revealed that many of these rocks have a significant normal-polarity overprint, as also noted by Opdyke et al. (1977) and Johnson et al. (1983). Examples of stepwise demagnetization are shown in Figure 10, which shows several types of behavior. Many specimens have very well-defined first- and second-removed magnetization directions (Fig. 10A) that allow clear and unambiguous definitions of their magnetic polarity. Sites where the majority of samples display this behavior are referred to as class A results. Many specimens have less well-defined second-removed components, due to either catastrophic disintegration of the rocks during thermal demagnetization (Fig. 10B) or a significant overlap in thermal or AF unblocking spectra, but for which polarity can be unambiguously determined by great-circle trends (Fig. 10C). Sites where the majority of samples displayed this behavior are referred to as class B sites. Several specimens have a combination of weak magnetization and poor demagnetization behavior (Fig. 10D), but a polarity of the last-removed magnetization can be safely inferred; sites where the majority of samples display this behavior are termed class C. Table DR1 (GSA supplementary material; see footnote 1) provides a complete list of site locations, polarities, and data quality.

Based on these results, we find good agreement between the polarity determined by the majority of our sample sites and those of Johnson et al. (1983). There were several cases where our results clearly indicated reversed polarity for the same or very similar stratigraphic levels that Johnson et al. (1983) determined to be normal polarity (see Table DR2; see footnote

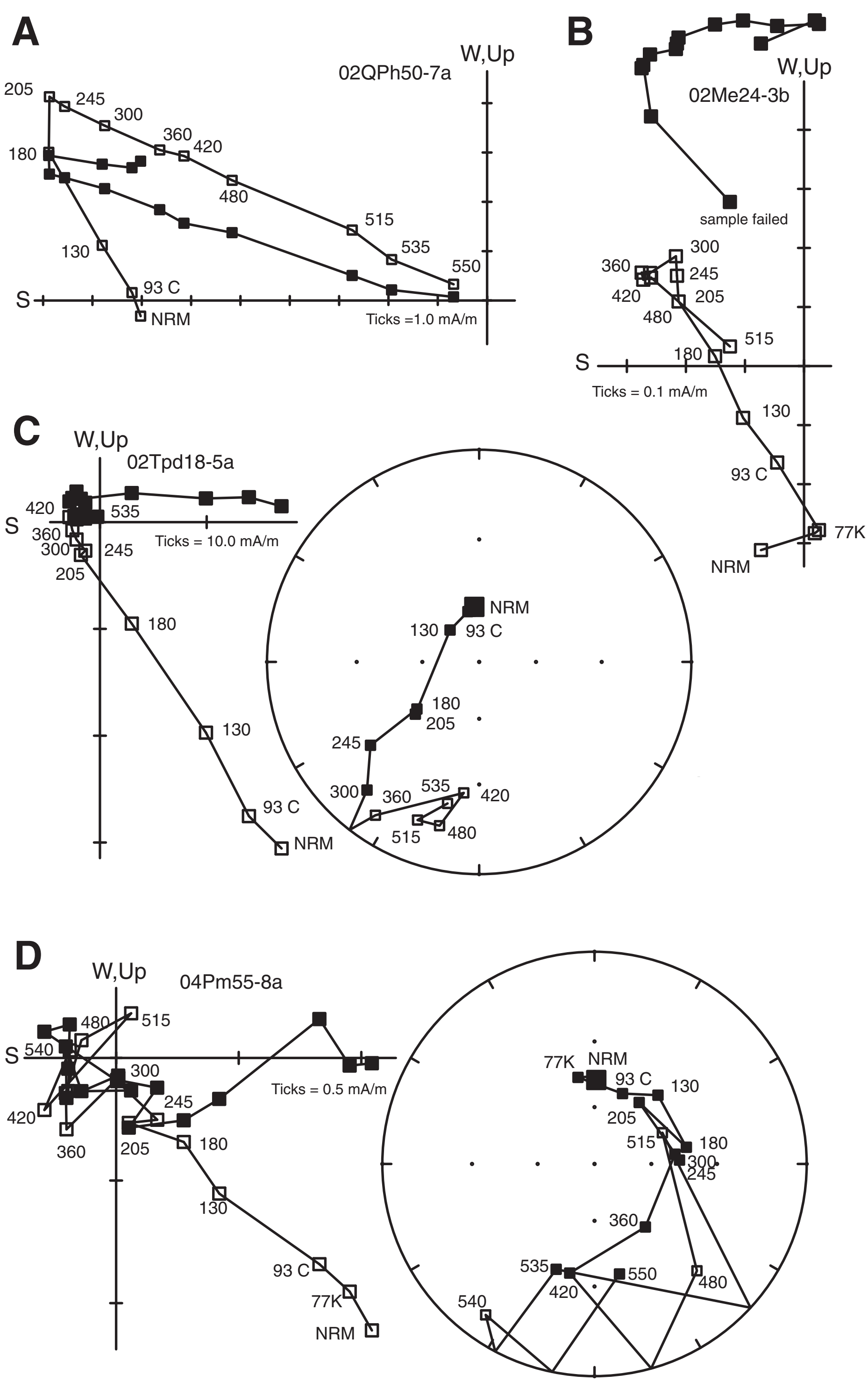

Figure 10. Examples of paleomagnetic results. For all orthogonal vector plots, open symbols denote projection of vector on the vertical plane, and filled symbols denote projection on the horizontal plane. Demagnetization steps are given in degrees C (77 K denotes liquid-nitrogen treatment step). For the stereographic (equal-angle) projections, filled symbols denote lower-hemisphere directions, and open symbols denote upper-hemisphere directions. (A) Orthogonal vector plot of a class A specimen with clear, linear magnetization components. (B) Orthogonal vector plot of a class B specimen that failed by catastrophic disintegration during heating, but still shows clearly defined polarity. (C) Orthogonal vector plot, and stereographic projection of a class B specimen with overlapping first- and second-removed magnetization components; polarity is well defined by great-circle trend of directions during demagnetization. (D) Orthogonal vector plot and stereographic projection of a class C specimen; although the magnetization is poorly defined, the polarity can be inferred by a combination of the vector and great-circle demagnetization trends. NRM— natural remanent magnetization.

1). We attribute this difference to the combined effects of the often difficult to remove normal-polarity overprint, and the single-step thermal treatment (with no vector or great-circle analysis), of Johnson et al.'s (1983) results. We also identified several sites reported in our prior work in the Split Mountain Gorge area (Dorsey et al., 2007) where revisions to the reported polarity are made in this study. These changes are attributed to a combination of sparse demagnetization data (1–2 samples in the study by Johnson et al., 1983), revisions in demagnetization treatments that led to better-defined results, and use of combined vector and great-circle trends to determine the polarity of the last-removed magnetization component. The end result is the delineation of 26 polarity reversals that are defined by 228 sites in the section (Fig. 5; Fig. DR1 [see footnote 1]).

Correlation of 26 magnetic reversals to the geomagnetic polarity time scale (GPTS; Cande and Kent, 1995; Gradstein et al., 2004) provides excellent control on the age of the section (Fig. 5). The reversals are hung from the GPTS using biostratigraphic placement of the Miocene-Pliocene boundary at 691 m in the section (Dorsey et al., 2007) and new U-Pb ages of the two tuffs at 4454 and 4488 m (2.65 ± 0.05 and 2.60 ± 0.06 Ma, this study). The resulting correlation to the GPTS is the only one that produces a reasonable chronology of sediment accumulation. Alternative correlations require extremely large, unreasonable spikes in sedimentation rate and violate independent age controls, and thus are rejected (Fig. 11). Our preferred chronology places the Miocene-Pliocene boundary at the position determined from marine microfossils (Dorsey et al., 2007), and it is consistent with prior results of Opdyke et al. (1977) and Johnson et al. (1983).

There is some uncertainty in the age of the lower part of the section (Fig. 5; Fig. DR1 [see footnote 1]). We infer that the thick reversed interval in the lower half of the Elephant Trees conglomerate member correlates to the lower part of the Gilbert magnetochron (7.09–7.34 or 7.43 Ma). One short-lived normal subchron (C3Br.1n; 3 k.y. duration) likely was missed between sample sites (Fig. 5). Our lowest reversed site, at the top of the lower sandstone member, most likely sits just above the top of subchron C4n.1n (7.43 Ma) or subchron C3Br.2n (7.34 Ma). This interpretation yields a nondecompacted sediment-accumulation rate of 0.4–0.5 mm/yr in the lower 130 m of the conglomerate member, consistent with rates calculated for the upper half of the Elephant Trees Formation. Because there is no age control in the lower sandstone member of the Elephant Trees Formation (Fig. 5), the age of the oldest sediment at the base of the section, east of Split Mountain Gorge, is estimated by extrapolating a nondecompacted sediment-accumulation rate of 0.2–0.5 mm/yr through the lower 140–190 m of section, and adding the range of possible durations to the inferred age of the lowest paleomagnetic collection site (7.34 or 7.43 Ma). This yields an age of 8.0 ± 0.4 Ma for the oldest deposits at the base of the section.

Our new data confirm that the change from normal to reversed polarity located 21 ± 13 m above the upper tuff is the Gauss-Matuyama boundary (2.58 Ma) (Fig. 5). Using present-day stratigraphic thicknesses, we calculate undecompacted sediment-accumulation rates of ~0.7 mm/yr between the two tuffs, and 1.0 mm/yr between the upper tuff and the Gauss-Matuyama reversal. These rates are similar to the average, longer-term nondecompacted accumulation rate of ~0.60 mm/yr calculated using magnetic reversals in this part of the section (Fig. 12).

SUBSIDENCE ANALYSIS

Figure 12 tracks 7 m.y. of subsidence in the Fish Creek–Vallecito basin, from ca. 8.0 to 0.95 Ma. This plot includes three curves for basin subsidence: one showing a plot of present-day thickness as a function of age (= nondecompacted subsidence), one for total subsidence calculated using the decompaction method described previously, and one for the component of total subsidence that is attributed to a tectonic driving force. All three curves are corrected for changes in global eustatic sea level using the curve of Hardenbol et al. (1998), and assume that nonmarine units accumulated at or close to sea level. The magnitude of eustatic change, albeit uncertain, is small relative to stratigraphic thickness, so the choice of a eustatic curve does not strongly affect the overall shape of the subsidence curve. The curve that uses present-day thickness does not include the effects of sediment compaction during burial and therefore is not an accurate subsidence history; it is included for comparison and completeness only. The curve for total subsidence tracks the depth to the base of the section through time and accounts for the effects of progressive sediment compaction with increasing burial depth. Tectonic subsidence is calculated by removing the effect of the sediment load assuming a local (Airy) isostatic response to loading, and the residual is assumed to be due to a tectonic driving force (Angevine et al., 1990). All three versions of the subsidence curve reveal a relatively simple four-part history of moderate (8.0–4.5 Ma) to fast (4.5–3.1 Ma) to moderate (3.1–0.95 Ma) subsidence, followed by post–1 Ma rapid uplift of the base of the section (Fig. 12).

The decompacted subsidence curves diverge into two lines in the marine part of the section (Fig. 12), reflecting uncertainty in paleo–water depth. Curves that assume a minimum paleobathymetry reveal relatively constant subsidence at a rate of 0.46 mm/yr (total) and 0.26 mm/yr (tectonic) between 8.0 and 4.5 Ma. In contrast, curves that assume the maximum paleobathymetry suggest a period of accelerated subsidence followed by rapid uplift between ca. 5.8 and 5.0 Ma, reflecting inferred large changes in paleo–water depth. While we cannot rule out the maximum estimate of paleobathymetry, we favor the minimum estimate because it is consistent with observed lithofacies, and it removes a short-lived pulse of uplift in the basin for which we have no other evidence and no obvious mechanism.

The plot in Figure 12 reveals an abrupt change at 4.5 Ma to rapid subsidence (2.11 mm/yr total rate; 0.85 mm/yr tectonic rate) that lasted for 1.4 m.y. until 3.1 Ma. The end of this segment is marked by a similarly abrupt return to moderate subsidence rate that lasted from 3.1 Ma to the end of basin subsidence at ca. 1 Ma. Since ca. 1 Ma, the entire basin has been inverted, uplifted, and deeply eroded, exposing the base of the section at elevations up to ~300 m above sea level around Split Mountain Gorge (Figs. 2 and 12).

DISCUSSION

The results of this study provide new insights into the subsidence history of the Fish Creek–Vallecito basin, crustal deformation related to development of the Pacific–North America plate boundary, chronology and dynamics of the Pliocene Colorado River, and the competing roles of subsidence and sediment supply in filling this large transtensional basin. We find that the base of the Elephant Trees Formation is 8.0 ± 0.4 Ma, the oldest marine deposits are 6.3 Ma, and Colorado River–derived sand first appears in this section at 5.3 Ma (Fig. 5), consistent with

Figure 11. Comparison of our preferred correlation to the geomagnetic polarity time scale (GPTS) with two alternative correlations. (A) Present-day stratigraphic height versus age. (B) Sediment-accumulation rates (using present-day thicknesses) versus age. The alternative correlations yield unreasonably large spikes in sediment-accumulation rate, and do not correctly correlate the Gauss-Matuyama reversal to the two dated tuffs at ~4500 m in the section (Fig. 5).

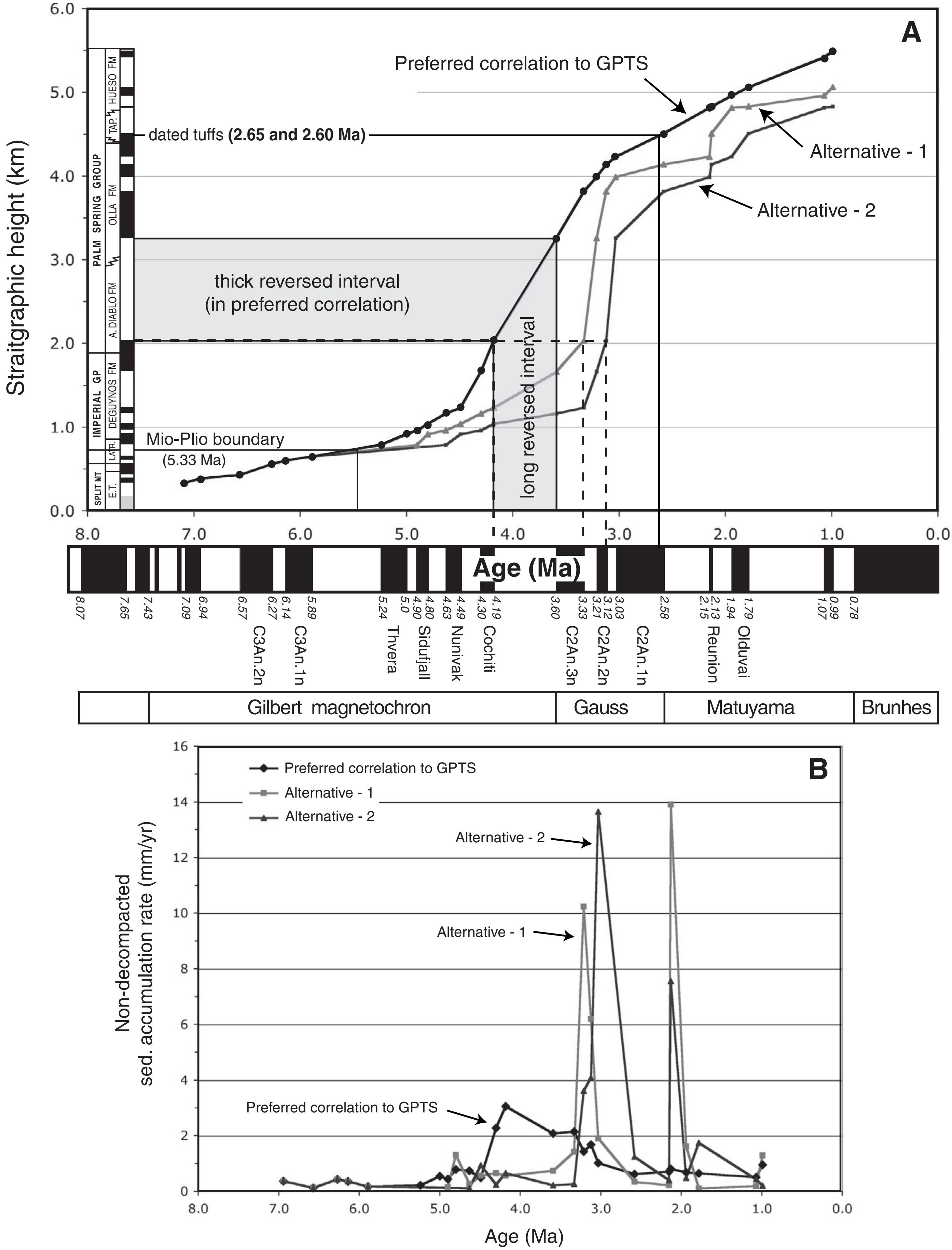
A
Preferred correlation to GPTS
Alternative - 1
Alternative - 2
dated tuffs (2.65 and 2.60 Ma)
thick reversed interval
(in preferred correlation)
long reversed interval
Mio-Plio boundary
(5.33 Ma)
Straitgraphic height (km)
PALM SPRING GROUP
IMPERIAL GP
SPLIT MT
HUESO FM
TAP.
OLLA FM
A. DIABLO FM
DEGUYNOS FM
LATR.
E.T.
Age (Ma)
C3An.2n
C3An.1n
Thvera
Sidufjall
Nunivak
Cochiti
C2An.3n
C2An.2n
C2An.1n
Reunion
Olduvai
Gilbert magnetochron
Gauss
Matuyama
Brunhes
B
Non-decompacted
sed. accumulation rate (mm/yr)
Age (Ma)

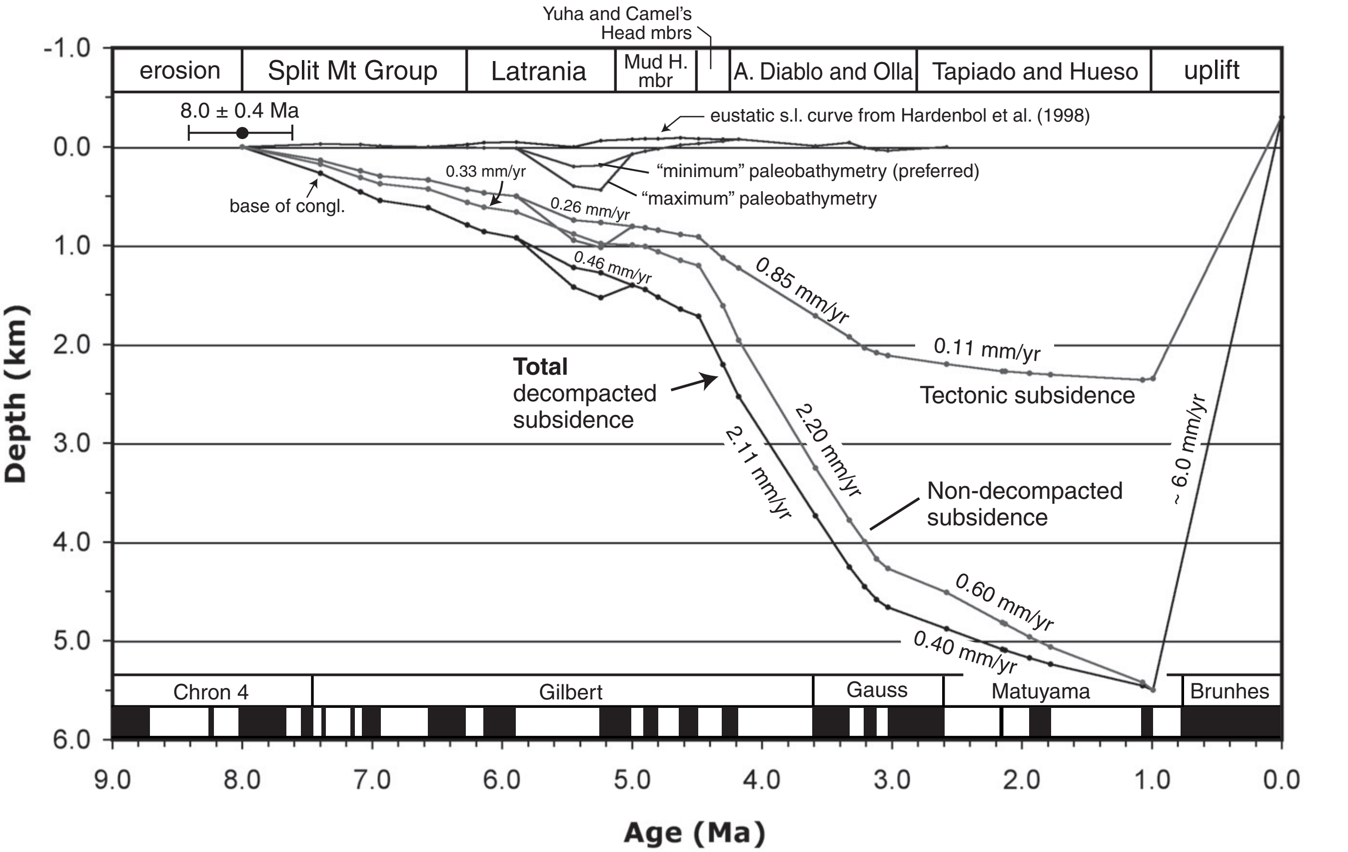

Figure 12. Subsidence curve for the Fish Creek–Vallecito basin, showing total decompacted subsidence, subsidence that would be calculated using present-day thicknesses, and tectonic subsidence (the component of subsidence due to a tectonic driving force). All three curves reveal a segmented, three-stage history of moderate to fast to moderate subsidence, from ca. 8.0 to 0.95 Ma.

the conclusions of Dorsey et al. (2007). Figure 12 tracks ~7 m.y. of crustal subsidence in response to tectonic driving forces and sediment loading, and provides new evidence for onset of rapid uplift and inversion at ca. 1 Ma.

Figure 13 presents paleogeographic reconstructions for the Salton Trough basin at 7–8, 6, 4, and 2 Ma. The reconstructions restore ~22 km of offset on the San Jacinto fault and ~10–15 km on the West Salton detachment fault (e.g., Sharp, 1967; Janecke et al., 2010; Shirvell et al., 2009), and build on previous reconstructions of this region (Winker and Kidwell, 1986; Matti and Morton, 1993). We assume an average slip rate of ~45–50 km/m.y. for the San Andreas fault prior to 1 Ma (DeMets and Dixon, 1999), and ~15–20 km/m.y. since ca. 1 Ma (e.g., van der Woerd et al., 2006), for a total Pacific–North America offset of ~290 km since 6 Ma (Oskin and Stock, 2003b). We restore an additional ~20–30 km to arrive at the reconstruction for ca. 7–8 Ma (Fig. 13A). Figure 14 presents the results of the stratigraphic analysis on a linear time scale to highlight the chronology of subsidence and deposition in the basin.

Onset of Deformation and the San Andreas Fault

The Cenozoic history of displacement on the Pacific–North America plate boundary in the Salton Trough and Gulf of California is widely debated, with prevailing models falling into two main groups. According to the first group of models, roughly 300 km of dextral translation has accumulated since ca. 6 Ma along the southern San Andreas fault system (Crowell, 1981; Ehlig, 1981; Nicholson et al., 1994; Ingersoll and Rumelhart, 1999) and Gulf of California (Gastil et al., 1973, 1991; Spencer and Normark, 1979; Stock and Hodges, 1989; Atwater and Stock, 1998; Oskin and Stock, 2003b). These studies conclude that prior to 6 Ma, relative plate motion was accommodated by dextral offset in the Los Angeles basin, offshore California borderland basins, and the Tosco-Abreojos fault west of Baja California. The second group of models proposes that relative plate motion began in the Gulf of California to Salton Trough corridor much earlier, initiating ca. 12–17 Ma and accumulating ~300–450 km of total offset (Powell, 1981, 1993; Powell and Weldon, 1992; Weldon et al., 1993; Matti and Morton, 1993; Gans, 1997; Fletcher et al., 2007). Many group-two models suggest ~160 km of post–6 Ma offset on the San Andreas fault in southern California, much less than the ~300 km inferred by the first group. Other workers have proposed that discrepancies in displacement magnitude between the two groups of models can be reconciled by including off-fault deformation and large-scale clockwise rotation (Dickinson, 1996; Dickinson and Wernicke, 1997; Axen, 2000). While the geometrical models provide useful insights, lack of consensus on the question of timing prevents a full understanding of the kinematic evolution of the Pacific–North America plate boundary.

Data presented herein record the onset of strong local extensional or transtensional deformation at Split Mountain Gorge by ca. 7.4 Ma (age of oldest conglomerate in the Elephant Trees Formation), likely starting ca. 8.0 ± 0.4 Ma (base of the lower sandstone member). Although boulder-bearing conglomerate provides the earliest direct evidence for structurally controlled steep topography at ca. 7.4 Ma, the

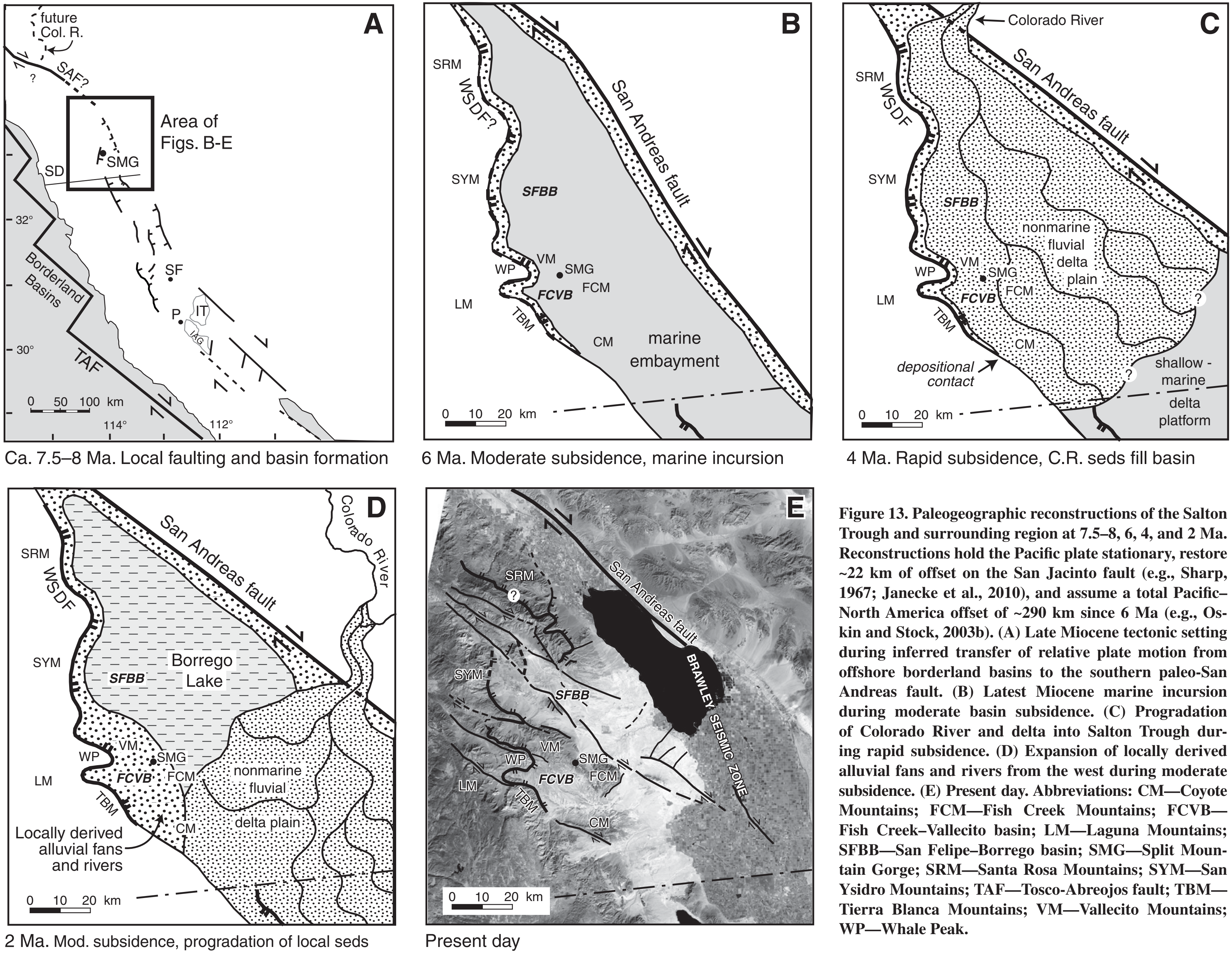

Figure 13. Paleogeographic reconstructions of the Salton Trough and surrounding region at 7.5–8, 6, 4, and 2 Ma. Reconstructions hold the Pacific plate stationary, restore ~22 km of offset on the San Jacinto fault (e.g., Sharp, 1967; Janecke et al., 2010), and assume a total Pacific–North America offset of ~290 km since 6 Ma (e.g., Oskin and Stock, 2003b). (A) Late Miocene tectonic setting during inferred transfer of relative plate motion from offshore borderland basins to the southern paleo-San Andreas fault. (B) Latest Miocene marine incursion during moderate basin subsidence. (C) Progradation of Colorado River and delta into Salton Trough during rapid subsidence. (D) Expansion of locally derived alluvial fans and rivers from the west during moderate subsidence. (E) Present day. Abbreviations: CM—Coyote Mountains; FCM—Fish Creek Mountains; FCVB—Fish Creek–Vallecito basin; LM—Laguna Mountains; SFBB—San Felipe–Borrego basin; SMG—Split Mountain Gorge; SRM—Santa Rosa Mountains; SYM—San Ysidro Mountains; TAF—Tosco-Abreojos fault; TBM—Tierra Blanca Mountains; VM—Vallecito Mountains; WP—Whale Peak.

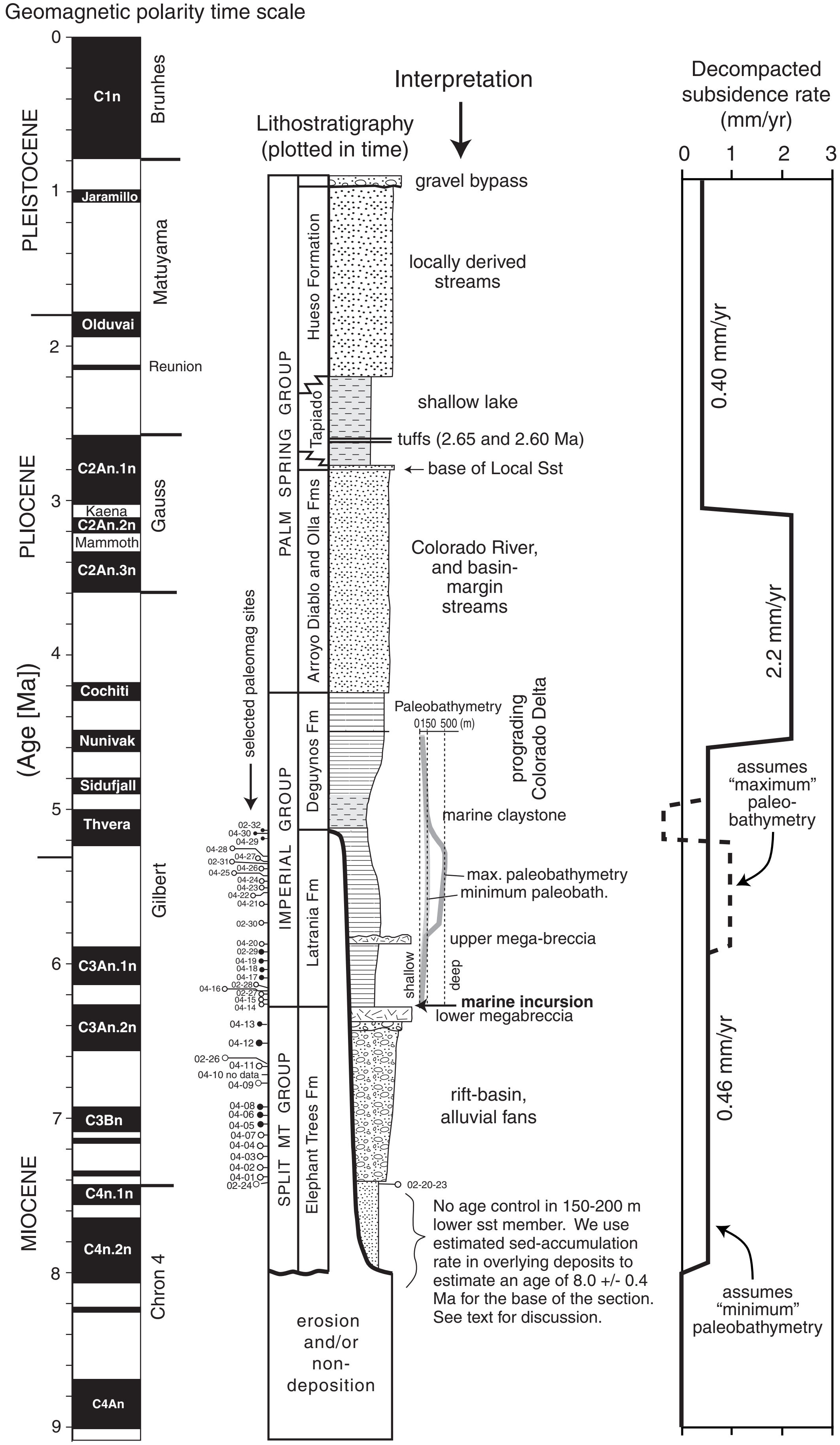
Geomagnetic polarity time scale
(Age [Ma])
PLEISTOCENE
PLIOCENE
MIOCENE
C1n
Brunhes
Jaramillo
Matuyama
Olduvai
Reunion
C2An.1n
Kaena
C2An.2n
Mammoth
C2An.3n
Gauss
Cochiti
Nunivak
Sidufjall
Thvera
Gilbert
C3An.1n
C3An.2n
C3Bn
C4n.1n
C4n.2n
Chron 4
C4An
Lithostratigraphy
(plotted in time)
Interpretation
PALM SPRING GROUP
Hueso Formation
Tapiado
Arroyo Diablo and Olla Fms
IMPERIAL GROUP
Deguynos Fm
Latrania Fm
SPLIT MT GROUP
Elephant Trees Fm
selected paleomag sites
gravel bypass
locally derived streams
shallow lake
tuffs (2.65 and 2.60 Ma)
base of Local Sst
Colorado River, and basin-margin streams
Paleobathymetry
0 150 500 (m)
prograding Colorado Delta
marine claystone
max. paleobathymetry
minimum paleobath.
upper mega-breccia
shallow
deep
marine incursion
lower megabreccia
rift-basin, alluvial fans
02-20-23
No age control in 150-200 m lower sst member. We use estimated sed-accumulation rate in overlying deposits to estimate an age of 8.0 +/- 0.4 Ma for the base of the section. See text for discussion.
erosion and/or non-deposition
Decompacted subsidence rate (mm/yr)
0.40 mm/yr
2.2 mm/yr
0.46 mm/yr
assumes "maximum" paleo-bathymetry
assumes "minimum" paleobathymetry

conformable nature of the lower Elephant Trees Formation east of Split Mountain Gorge indicates that the lower sandstone member likely accumulated in a tectonically active basin starting ca. 8.0 ± 0.4 Ma. We speculate that the onset of local deformation may reflect initiation of off-fault strain adjacent to the paleo–San Andreas fault when it became established as the Pacific–North America plate boundary in the Salton Trough at ca. 7–8 Ma (Fig. 13A). This coincides temporally with—and may have been linked to—a change to a more strike-slip relative plate motion at ca. 8 Ma (Atwater and Stock, 1998), though newer analyses do not indicate a change in plate motion at this time (Wilson et al., 2005). Alternatively, the onset of deformation in this area could represent intraplate strain prior to establishment of the Pacific–North America plate boundary in the Salton Trough at ca. 6 Ma, or it could be off-fault strain that started long after initiation of the paleo–San Andreas fault around 12–17 Ma. We favor the first hypothesis—onset of local deformation due to initiation of the paleo–San Andreas fault—because the present-day San Andreas fault is embedded in a wide belt of deformation, and the study area restores to a position close to the paleo–San Andreas fault in the reconstruction (Fig. 13A). While we cannot rule out the possibility that the paleo–San Andreas fault was present NE of the Salton Trough before the onset of deformation at Split Mountain Gorge, the overlying marine deposits and correlation to other distant localities provide clear evidence that the plate boundary was established in the Salton Trough by or before 6.3 Ma (see following).

Our conclusion that local transtensional deformation started at ca. 8.0 ± 0.4 Ma differs from a recent study of (U-Th)/He cooling ages in the lower plate of the West Salton detachment fault (Shirvell et al., 2009), which suggested that exhumation due to slip on the detachment fault may have started as early as ca. 12 Ma. However, Shirvell et al. (2009) did not consider long-term cooling due to a regional thermal event—perhaps related to development of a slab window east of the San Andreas transform boundary (e.g., Dickinson and Snyder, 1979; Severinghaus and Atwater, 1990; Wilson et al., 2005)—as an alternative explanation for the data. The cause of slow cooling since ca. 25 Ma north of Split Mountain Gorge in the eastern Peninsular Ranges (Luther et al., 2008) is similarly enigmatic. We propose that, in contrast to ambiguous results emerging from thermochronologic studies, stratigraphy provides a robust, well-dated record of crustal deformation in this area, and that there is no compelling evidence for major extensional or transtensional deformation in the Fish Creek–Vallecito basin prior to ca. 8 Ma. Suggestions that an older stratigraphic record resides concealed in the subsurface are untenable because the latest Miocene and Pliocene base of the section is well exposed in numerous places due to young uplift and exhumation. Because the Salton Trough has opened by lithospheric rupture and spreading (e.g., Fuis et al., 1984), the study area restores to a position close to the paleo–San Andreas fault (Fig. 13A), making it unlikely that a deep older section is preserved at depth in the subsurface of the modern Salton Trough. We therefore conclude that crustal extension or transtension in the western Salton Trough began at ca. 7.5–8 Ma, and that older (U-Th)/He ages in the footwall of the West Salton detachment fault most likely record the younger part of a protracted regional cooling history that began in middle Tertiary time.

Figure 14. Chronostratigraphic summary of the Fish Creek–Vallecito basin showing lithostratigraphy, subsidence rates, and inferred paleobathymetry for the marine Imperial Group (Dorsey et al., 2007; this study), plotted as a function of time. Paleomagnetic sample sites and polarities are shown for the lower part of the section, where scale permits. Additional details of sample locations are provided in the GSA Data Repository online supplement (Fig. DR1; see text footnote 1).

Late Miocene Marine Incursion

The oldest marine deposits at Split Mountain Gorge, dated here at ca. 6.3 Ma, record late Miocene marine flooding into the Salton Trough (Fig. 13B). Subsidence rate in the basin was moderate and more or less constant from ca. 8.0 to 4.5 Ma (Fig. 12), so it is unlikely that marine incursion resulted from an abrupt increase in subsidence rate at 6.3 Ma. Thus, it is tempting to attribute this event to a late Miocene rise in global sea level (e.g., Haq et al., 1987; Hardenbol et al., 1998) superimposed on long-term tectonic subsidence. However, recent reconstructions of global sea level based on refined stratigraphic analysis and backstripping methods do not reveal a large-magnitude change in global sea level in late Miocene time (Van Sickel et al., 2004; Miller et al., 2005). Large discrepancies between published sea-level curves, combined with possible complications related to slab-window thermal effects (e.g., Wilson et al., 2005) and dynamic topography (Moucha et al., 2008; Spasojevic et al., 2008), currently make it impossible to assess the possible influence of eustatic sea-level change on this event.

Despite the uncertain role of late Miocene eustatic sea level, the regional distribution of marine sediments places a useful constraint on the timing of plate-boundary deformation. Marine deposits of remarkably similar age (ca. 6.3–6.5 Ma) are preserved in a narrow, ~600-km-long belt from Isla Tiburon in the south (Oskin et al., 2001; Oskin and Stock, 2003a) to the northern Salton Trough and southern San Bernardino Mountains (Rymer et al., 1994, 1995; McDougall et al., 1999; McDougall, 2008). In most localities, late Miocene marine deposits conformably overlie nonmarine deposits that themselves rest nonconformably on Cretaceous or older plutonic rock. This suggests that these localities were either uplifting or neutral until a structural change caused subsidence and deposition in nonmarine environments, which subsequently were inundated by marine water. The similar timing of these events along a 600-km-long narrow belt provides clear evidence that the Pacific–North America plate boundary was established along the Salton Trough–Gulf of California corridor by the time of marine incursion. We infer that local deformation at Split Mountain Gorge and elsewhere was replaced by regionally integrated extension and transtension along the plate boundary, which caused crustal thinning and lowering of topography to sea level and culminated in marine flooding at ca. 6.3–6.5 Ma.

Controls on Segmented Basin Subsidence

As noted already, the subsidence history for the Fish Creek–Vallecito basin consists of three linear segments with abrupt changes in rate from moderate (0.46 mm/yr) to fast (2.11 mm/yr) to moderate (0.40 mm/yr), followed by rapid uplift and exhumation (Fig. 5). This is not predicted for rift basins, which typically show a gradual decay of subsidence rate in response to lithospheric cooling (McKenzie, 1978; Sclater and Christie, 1980; Bond et al., 1983). Instead, the second two stages of subsidence are reminiscent of strike-slip–related basins, such as the Miocene-Pliocene Ridge Basin (Crowell and Link, 1982; Christie-Blick and Biddle, 1985) and Pliocene Loreto basin (Dorsey and Umhoefer, 2000), which experience an early stage of rapid subsidence followed by an abrupt change to slower subsidence (see also Xie and Heller, 2009). Pitman and Andrews (1985) proposed that the segmented subsidence pattern of transtensional strike-slip basins results from significant heat loss during rifting, with much slower postrift subsidence due to little heat loss after the end of the rift phase. Karner and Dewey (1986) suggested that the presence of a subhorizontal midcrustal detachment leads to thinning of the crust without involvement of the mantle lithosphere, thus maximizing subsidence rate during rifting. Segmented subsidence histories also result from geometric complexities and changes in fault geometry and slip rate as rocks enter and exit bends and steps in strike-slip fault systems. Such changes typically occur in strike-slip fault zones over short time scales (Mann et al., 1983; Dickinson et al., 1987; Machette et al., 1991, 1992; McCalpin and Nishenko, 1996) and have been documented north of the Fish Creek–Vallecito basin in smaller Pleistocene strike-slip basins (Lutz et al., 2006; Kirby et al., 2007; Belgarde, 2007; Steely et al., 2009).

In the Fish Creek–Vallecito basin, temporal changes in subsidence rate likely reflect changes in slip rate on basin-bounding faults, and may record initiation of the West Salton detachment fault as early as 8.0 ± 0.4 Ma or as late as ca. 4.5 Ma. Onset of lithospheric rupture and voluminous mafic intrusions in the Salton Trough (e.g., Fuis et al., 1984) may have also played a role. Although a specific driving mechanism cannot be isolated, the segmented subsidence curve in Figure 12 suggests evolving deformation adjacent to geometrically complex transtensional faults in a regional strike-slip–related fault system. This conclusion is consistent with our general understanding that Pliocene subsidence and deposition took place during translation along the San Andreas fault at the northeast margin of the basin (Figs. 1 and 13; Axen and Fletcher, 1998).

Progradation and Basin Filling by the Colorado Delta

During early Pliocene time, the Colorado River produced a large volume of sediment that filled the Salton Trough up to sea level, forcing progradation of the fluvial delta plain southeast into the northern Gulf of California (Fig. 13C). Up-section coarsening through the upper Mud Hills, Yuha, and Camels Head Members (Fig. 5) records progradation of the Colorado River delta into the basin from ca. 4.9 to 4.2 Ma. The base of the Arroyo Diablo Formation signals arrival of the fluvial part of the system at 4.25 Ma. It is significant that the delta prograded into this area continuously during an abrupt fourfold increase in subsidence rate at ca. 4.5 Ma (Fig. 12). If other parameters (sea level, climate, rate of sediment input) are held constant, an increase in subsidence rate should cause retrogradation and retreat of a delta, which would produce an up-section decrease in grain size and change to more distal deposits (e.g., Paola et al., 1992; Heller and Paola, 1992), opposite of the documented coarsening-up trend.

The observation that delta progradation took place during accelerated subsidence, and that fluvial conditions persisted for 1.4 m.y. during the rapid-subsidence phase, provides evidence that a large increase in sediment flux to the basin at 4.9–4.6 Ma overwhelmed the competing effect of increased subsidence rate, which otherwise would have caused coastal transgression and a decrease in the size of the delta (e.g., Van Wagoner et al., 1990; Posamentier et al., 1988; Muto and Steel, 1992, 2001, 2002). This kind of behavior—strong delta progradation during increased production of accommodation space—has been observed elsewhere and is used to document the occurrence and significance of supply-driven deltas (e.g., Goodbred and Kuehl, 2000; Carvajal and Steel, 2006; Porebski and Steel, 2006).

Basin Inversion and Uplift

The Fish Creek–Vallecito basin is well exposed because the section has been uplifted, tilted, and eroded during the past ~1 m.y. The onset of tilting is dated at ca. 1.2 Ma based on a zone of fanning dips that begins just below the base of the Jaramillo subchron (1.07 Ma; Fig. 5). Basin subsidence and sediment accumulation had ended by ca. 0.95 Ma. We infer that post–1 Ma tilting is currently taking place in a large tilt block bounded by the Elsinore fault on the southwest and the Fish Creek Mountains fault on the northeast (Fig. 2). Because stratigraphic thickness likely represents total depth of the basin, and the base of the section is now exposed at ~300 m elevation, we conclude that there has been as much as 5.7 km of uplift in the Fish Creek Mountains since 0.95 Ma, at an average rate of ~6 mm/yr. The amount of uplift decreases to the southwest and approaches zero to slight subsidence close to the Elsinore fault (Fig. 2). The change from widespread subsidence to uplift and basin inversion resulted from initiation of the Elsinore and other strike-slip faults in the western Salton Trough at ca. 1.1–1.3 Ma (Johnson et al., 1983; Lutz et al., 2006; Kirby et al., 2007; Steely et al., 2009; Janecke et al., 2010; this study). Onset of this new structural style represents a major, relatively recent tectonic reorganization and southwestward widening of the San Andreas fault system.

CONCLUSIONS

A 5.5-km-thick stratigraphic section exposed in the Fish Creek–Vallecito basin provides a high-fidelity record of sedimentation, subsidence, basin filling, and uplift from late Miocene time to the present. Geohistory analysis reveals a segmented history of: (1) moderate subsidence from 8.0 to 4.5 Ma; (2) rapid subsidence from 4.5 to 3.1 Ma; (3) moderate subsidence from 3.1 to 0.95 Ma; and (4) tilting and rapid uplift and erosion since ca. 1 Ma. The strongly segmented nature of the subsidence history is likely related to changes in slip rate and slip partitioning on basin-bounding faults, in particular the low-angle West Salton detachment fault on the west and the San Andreas fault on the northeast.

The onset of subsidence and deposition at ca. 8.0 ± 0.4 Ma resulted from onset of local extensional or transtensional deformation, and may record initiation of the paleo–San Andreas fault when it became established as the Pacific–North America plate boundary in the Salton Trough. Alternatively, plate-boundary strain could have initiated in the Salton Trough region prior to or after the onset of deformation in this area, but no later than 6.3 Ma (age of widespread marine incursion). The age of the West Salton detachment fault remains uncertain, and could be as old as ca. 8.0 or as young as 4.5 Ma (age of abrupt increase in subsidence rate).

Large-scale progradation of the Colorado delta into the basin took place during an abrupt increase in subsidence rate at ca. 4.5 Ma, and fluvial-deltaic conditions persisted for 1.4 m.y. during the rapid-subsidence phase. This behavior contradicts the predictions of subsidence-driven stratigraphic models because, if other parameters are held constant, a change to rapid subsidence should cause retreat and retrogradation of a delta, not progradation. We therefore infer that Pliocene progradation of the delta resulted from a large increase in sediment input from the Colorado River that overwhelmed the competing influence of rapid subsidence.

Rapid uplift, inversion, and erosion of the basinal succession began at ca. 1 Ma in response to initiation of currently active strike-slip faults and dextral wrench deformation in the western Salton Trough. Complex segmentation and destruction of the formerly intact supradetachment basin reflect profound, relatively recent reorganization of the San Andreas fault system.

ACKNOWLEDGMENTS

This study was supported by grants from the National Science Foundation to Dorsey (EAR-0838119), Housen (EAR- 0838167), and Janecke (EAR-0125497). The Cryogenic magnetometer at Western Washington University was provided by NSF grant EAR-9727032 to Housen. We thank George Jefferson and Mark Jorgenson for permits for field work in Anza-Borrego Desert State Park. Gary Petro, Jim Smith, and many volunteers from the Stout Paleontology Laboratory assisted with field work. L. Louise Gee helped with Arc-GIS data, and Everett Lindsay kindly shared unpublished notes from previous studies. This research benefited from discussions with Pat Abbott, Gary Axen, George Jefferson, Susan Kidwell, Kris McDougall, Lyn Murray, Mike Oskin, Tom Peryam, Catherine Shirvell, and Charlie Winker, and from reviews by Nick Christie-Blick, Cari Johnson, Paul Mann, and Jonathan Matti. We thank Burnie and Karen Burnworth for their kind hospitality and shelter at "El Rancho not so Grande" at the top of the section, and Eric Mustonen for housing and generous support in Borrego Springs.

REFERENCES CITED

Abbott, P.L., Kerr, D.R., Borron, S.E., Washburn, J.L., and Rightmer, D.A., 2002, Neogene sturzstrom deposits, Split Mountain area, Anza-Borrego Desert State Park, California, *in* Evans, S.G., and DeGraff, J.V., eds., Catastrophic Landslides: Effects, Occurrence, and Mechanisms: Geological Society of America, Reviews in Engineering Geology, v. 15, p. 379–400.

Angevine, C.L., Heller, P.L., and Paola, C., 1990, Quantitative Sedimentary Basin Modeling: American Association of Petroleum Geologists (AAPG) Short Course Note Series 32, 247 p.

Atwater, T., and Stock, J.M., 1998, Pacific–North America plate tectonics of the Neogene southwestern United States: An update: International Geology Review, v. 40, p. 375–402, doi: 10.1080/00206819809465216.

Axen, G.J., 2000, New palinspastic reconstructions of the southern San Andreas fault system and northern Gulf of California at 2, 4, 6.5, and 12 Ma: Eos (Transactions, American Geophysical Union), v. 81, no. 48, Fall Meeting supplement, abstract T22F–07.

Axen, G.J., and Fletcher, J.M., 1998, Late Miocene–Pleistocene extensional faulting, northern Gulf of California, Mexico and Salton Trough, California: International Geology Review, v. 40, p. 217–244, doi: 10.1080/00206819809465207.

Belgarde, B.E., 2007, Structural Characterization of the Three Southeast Segments of the Clark Fault, Salton Trough, California [M.S thesis]: Logan, Utah, Utah State University, 4 plates, map scale 1:24,000, 216 p.

Bialas, R.W., and Buck, W.R., 2009, How sediment promotes narrow rifting: Application to the Gulf of California: Tectonics, v. 28, doi: 10.1029/2008TC002394.

Black, L.P., Kamo, S.L., Williams, I.S., Mundil, R., Davis, D.W., Korsch, R.J., and Foudoulis, C., 2003, The application of SHRIMP to Phanerozoic geochronology; a critical appraisal of four zircon standards: Chemical Geology, v. 200, p. 171–188, doi: 10.1016/S0009-2541(03)00166-9.

Bond, G.C., Kominz, M.A., and Devlin, W.J., 1983, Thermal subsidence and eustasy in the lower Palaeozoic miogeocline of western North: American Naturalist, v. 306, p. 775–779.

Cande, S.C., and Kent, D.V., 1995, Revised calibration of the geomagnetic polarity timescale for the Late Cretaceous and Cenozoic: Journal of Geophysical Research, ser. B, Solid Earth and Planets, v. 100, p. 6093–6095.

Carvajal, C.R., and Steel, R.J., 2006, Thick turbidite successions from supply-dominated shelves during sea-level highstand: Geology, v. 34, p. 665–668, doi: 10.1130/G22505.1.

Cassiliano, M.J., 1999, Biostratigraphy of Blancan and Irvingtonian mammals in the Fish Creek–Vallecito section, southern California, and a review of the Blancan-Irvingtonian boundary: Journal of Vertebrate Paleontology, v. 19, p. 169–186.

Christie-Blick, N., and Biddle, K.T., 1985, Deformation and basin formation along strike-slip faults, *in* Biddle, K.T., and Christie-Blick, N., eds., Strike-Slip Deformation, Basin Formation, and Sedimentation: Society of Economic Paleontologists and Mineralogists Special Publication 37, p. 1–34.

Compton, R.R., 1985, Geology in the Field: New York, John Wiley, 398 p.

Crowell, J.C., 1981, An outline of the tectonic history of southeastern California, *in* Ernst, W.G., ed., The Geotectonic Development of California, Rubey Volume 1: Englewood Cliffs, New Jersey, Prentice-Hall, p. 583–600.

Crowell, J.C., ed., 2003, Evolution of Ridge Basin, Southern California: An Interplay of Sedimentation and Tectonics: Geological Society of America Special Paper 367, 247 p.

Crowell, J.C., and Link, M.H., eds., 1982, Geologic History of Ridge Basin, Southern California: Los Angeles, California, Pacific Section, Society of Economic Paleontologists and Mineralogists, 304 p.

DeMets, C., and Dixon, T.H., 1999, New kinematic models for Pacific–North America motion from 3 Ma to present: I. Evidence for steady motion and biases in the NUVEL-1A model: Geophysical Research Letters, v. 26, p. 1921–1924, doi: 10.1029/1999GL900405.

Dibblee, T.W., Jr., 1954, Geology of the Imperial Valley region, California, *in* Jahns, R.H., ed., Geology of Southern California: California Division of Mines Bulletin 170, p. 21–28.

Dibblee, T.W., Jr., 1984, Stratigraphy and tectonics of the San Felipe Hills, Borrego Badlands, Superstition Hills, and vicinity, *in* Rigsby, C.A., ed., The Imperial Basin—Tectonics, Sedimentation, and Thermal Aspects: Los Angeles, California, Pacific Section, Society of Economic Paleontologists and Mineralogists, p. 31–44.

Dibblee, T.W., Jr., 1996, Stratigraphy and tectonics of the Vallecito–Fish Creek Mountains, Vallecito Badlands, Coyote Mountains, and Yuha Desert, southwestern Imperial Basin, *in* Abbott, P.L., and Seymour, D.C., eds., Sturzstroms and Detachment Faults, Anza-Borrego Desert State Park, California: Santa Ana, California, South Coast Geological Society, Annual Field Trip Guide Book, v. 24, p. 59–80.

Dickinson, W.R., 1996, Kinematics of Transrotational Tectonism in the California Transverse Ranges and its Contribution to Cumulative Slip along the San Andreas Transform Fault System: Geological Society of America Special Paper 305, 46 p.

Dickinson, W.R., and Snyder, W.S., 1979, Geometry of subducted slabs related to San Andreas transform: The Journal of Geology, v. 87, p. 609–627, doi: 10.1086/628456.

Dickinson, W.R., and Wernicke, B.P., 1997, Reconciliation of San Andreas slip discrepancy by a combination of interior Basin and Range extension and transrotation near the coast: Geology, v. 25, p. 663–665, doi: 10.1130/0091-7613(1997)025<0663:ROSASD>2.3.CO;2.

Dickinson, W.R., Armin, R.A., Beckvar, N., Goodlin, T.C., Janecke, S.U., Mark, R.A., Norris, R.D., Radel, G., and Wortman, A.A., 1987, Geohistory analysis of rates of sediment accumulation and subsidence for selected California basins, *in* Ingersoll, R.V., and Ernst, W.G., eds., Cenozoic Basin Development of Coastal California; Rubey Volume VI: Englewood Cliffs, New Jersey, Prentice-Hall, p. 1–23.

Dorsey, R.J., 2006, Stratigraphy, tectonics, and basin evolution in the Anza-Borrego Desert region, *in* Jefferson, G.T., and Lindsay, L.E., eds., Fossil Treasures of Anza-Borrego Desert: San Diego, California, Sunbelt Publications, p. 89–104.

Dorsey, R.J., 2010, Sedimentation and crustal recycling along an active oblique-rift margin: Salton Trough and northern Gulf of California: Geology, v. 38, p. 443–446.

Dorsey, R.J., and Axen, G.J., 2009, End of detachment faulting and initiation of strike-slip faults at 1.0 Ma, western Fish Creek–Vallecito basin, southern California: Geological Society of America Abstracts with Programs, v. 41, no. 7, p. 138.

Dorsey, R.J., and Umhoefer, P.J., 2000, Tectonic and eustatic controls on sequence stratigraphy of the Pliocene Loreto basin, Baja California Sur, Mexico: Geological Society of America Bulletin, v. 112, p. 177–199, doi: 10.1130/0016-7606(2000)112<177:TAECOS>2.0.CO;2.

Dorsey, R.J., and Umhoefer, P.J., 2010, Influence of sediment input and plate-motion obliquity on basin development along an active oblique-divergent plate boundary: Gulf of California and Salton Trough, *in* Busby, C., and Azor, A., eds., Recent Advances in Tectonics of Sedimentary Basins: Wiley-Blackwell (in press).

Dorsey, R.J., Fluette, A., McDougall, K.A., Housen, B.A., Janecke, S.U., Axen, G.J., and Shirvell, C.R., 2007, Chronology of Miocene-Pliocene deposits at Split Mountain Gorge, southern California: A record of regional tectonics and Colorado River evolution: Geology, v. 35, p. 57–60, doi: 10.1130/G23139A.1.

Ehlig, P.L., 1981, Origin and tectonic history of the basement terrane of the San Gabriel Mountains, central Transverse Ranges, *in* Ernst, W.G., eds., The Geotectonic Development of California; Rubey Volume 1: Englewood Cliffs, New Jersey, Prentice-Hall, p. 253–283.

Elders, W.A., and Sass, J.H., 1988, The Salton Sea scientific drilling project: Journal of Geophysical Research, v. 93, no. B11, p. 12,953–12,968, doi: 10.1029/JB093iB11p12953.

Fletcher, J.M., Grove, M., Kimbrough, D., Lovera, O., and Gehrels, G.E., 2007, Ridge-trench interactions and the Neogene tectonic evolution of the Magdalena shelf and southern Gulf of California: Insights from detrital zircon U-Pb ages from the Magdalena fan and adjacent areas: Geological Society of America Bulletin, v. 119, p. 1313–1336, doi: 10.1130/B26067.1.

Fuis, G.S., Mooney, W.D., Healy, J.H., McMechan, G.A., and Lutter, W.J., 1984, A seismic refraction survey of the Imperial Valley region, California: Journal of Geophysical Research, v. 89, p. 1165–1189, doi: 10.1029/JB089iB02p01165.

Gans, P.B., 1997, Large-magnitude Oligo-Miocene extension in southern Sonora: Implications for the tectonic evolution of northwest Mexico: Tectonics, v. 16, p. 388–408, doi: 10.1029/97TC00496.

Gastil, R.G., Lemone, D.V., and Stewart, W.J., 1973, Permian fusulinids from near San Felipe, Baja California: The American Association of Petroleum Geologists Bulletin, v. 57, p. 746–747.

Gastil, R.G., Miller, R.H., Anderson, P., Crocker, J., Campbell, M., Buch, P., Lothringer, C., Leier-Engeldardt, P., DeLattre, M., Hoobs, J., and Roldan-Quintana, J., 1991, The relation between the Paleozoic strata on opposite sides of the Gulf of California, *in* Perez-Segura, E., and Jacques-Ayala, C., eds., Studies of Sonoran Geology: Geological Society of America Special Paper 254, p. 7–16.

Gastil, R.G., Kimbrough, D.L., and Abbott, P.L., 1996, Arrival of the Colorado River in the Salton Trough defined by magnetic susceptibility, *in* Abbott, P.L., and Seymour, D.C., eds., Sturzstroms and Detachment Faults, Anza-Borrego Desert State Park, California: Santa Ana, California, South Coast Geological Society, p. 203–207.

González-Fernández, A., Dañobeitia, J.J., Delgado-Argote, L.A., Michaud, F., Córdoba, D., and Bartolomé, R., 2005, Mode of extension and rifting history of upper Tiburón and upper Delfín basins, northern Gulf of California: Journal of Geophysical Research, v. 110, p. B01313, doi: 10.1029/2003JB002941.

Goodbred, S.L., and Kuehl, S.A., 2000, The significance of large sediment supply, active tectonism, and eustasy on margin sequence development: Late Quaternary stratigraphy and evolution of the Ganges–Brahmaputra delta: Sedimentary Geology, v. 133, p. 227–248, doi: 10.1016/S0037-0738(00)00041-5.

Gradstein, F., Ogg, J.G., and Smith, A.G., eds., 2004, A Geologic Time Scale: Cambridge, UK, Cambridge University, 610 p.

Hanna, G.D., 1926, Paleontology of Coyote Mountain, Imperial County, California: Proceeding of the California Academy of Sciences, fourth series, v. 14, p. 427–503.

Haq, B.U., Hardenbol, J., and Vail, P.R., 1987, Chronology of fluctuating sea levels since the Triassic: Science, v. 235, p. 1156–1167, doi: 10.1126/science.235.4793.1156.

Hardenbol, J., Thierry, J., Farley, M.B., Jacquin, T., de Graciansky, P.C., and Vail, P.R., 1998, Mesozoic and Cenozoic sequence chronostratigraphic framework, *in* de Graciansky, P.C., Hardenbol, J., Jacquin, T., and Vail, P.R., eds., Mesozoic and Cenozoic Sequence Stratigraphy of European Basins: Society for Sedimentary Geology, Special Publication 60 (Charts), p. 3–13.

Heller, P.L., and Paola, C., 1992, The large-scale dynamics of grain-size variation in alluvial basins: 2. Application to syntectonic conglomerate: Basin Research, v. 4, p. 91–102.

Herzig, C.T., Mehegan, J.M., and Stelting, C.E., 1988, Lithostratigraphy of the State 2–14 Borehole; Salton Sea Scientific Drilling Project: Journal of Geophysical Research, v. 93, p. 12,969–12,980, doi: 10.1029/JB093iB11p12969.

Housen, B.A., Dorsey, R.J., Janecke, S.U., and Axen, G.J., 2005, Rotation of Plio-Pleistocene sedimentary rocks in the Fish Creek–Vallecito Basin, western Salton Trough, CA: Eos (Transactions, American Geophysical Union), v. 86, no. 52, Fall Meeting supplement, abstract GP13A–0039.

Housen, B.A., Dorsey, R.J., Janecke, S.U., and Axen, G.J., 2006, Evolution of rotations in the Fish Creek–Vallecito basin, western Salton Trough, CA: Eos (Transactions, American Geophysical Union), v. 87, no. 52, Fall Meeting supplement, abstract T41D–1601.

Ingersoll, R.V., and Rumelhart, P.E., 1999, Three-stage evolution of the Los Angeles basin, southern California: Geology, v. 27, p. 593–596, doi: 10.1130/0091-7613(1999)027<0593:TSEOTL>2.3.CO;2.

Janecke, S.U., Dorsey, R.J., Forand, D., Steely, A.N., Kirby, S.M., Lutz, A.T., Housen, B.A., Belgarde, B., Langenheim, V.E., and Rittenour, T.M., 2010, High Geologic Slip Rates since Early Pleistocene Initiation of the San Jacinto and San Felipe Fault Zones in the San Andreas Fault System: Southern California, USA: Geological Society of America Special Paper 475, 48 p., doi:10.1130/2010.2475.

Jefferson, G.T., and Lindsay, L.E., eds., 2006, Fossil Treasures of Anza-Borrego Desert: San Diego, California, Sunbelt Publications, 394 p.

Johnson, N.M., Officer, C.B., Opdyke, N.D., Woodard, G.D., Zeitler, P.K., and Lindsay, E.H., 1983, Rates of late Cenozoic tectonism in the Vallecito–Fish Creek basin, western Imperial Valley: California Geology, v. 11, p. 664–667.

Kairouz, M.E., 2005, Geology of the Whale Peak Region of the Vallecito Mountains: Emphasis on the Kinematics and Timing of the West Salton Detachment Fault, Southern California [M.S. thesis]: Los Angeles, University of California, 156 p.

Karner, G.D., and Dewey, J.F., 1986, Rifting, lithospheric versus crustal extension as applied to the Ridge Basin of southern California, *in* Halbouty, M.E., ed., Future Petroleum Provinces of the World: American Association of Petroleum Geologists Memoir 40, p. 317–337.

Kerr, D.R., 1982, Early Neogene Continental Sedimentation, Western Salton Trough, California [M.S. thesis]: San Diego, California, San Diego State University, 138 p.

Kerr, D.R., and Abbott, P.L., 1996, Miocene subaerial sturzstrom deposits, Split Mountain, Anza-Borrego Desert State Park, *in* Abbott, P.L., and Seymour, D.C., eds., Sturzstroms and Detachment Faults, Anza-Borrego Desert State Park, California: Santa Ana, California, South Coast Geological Society, p. 149–163.

Kerr, D.R., and Kidwell, S.M., 1991, Late Cenozoic sedimentation and tectonics, western Salton Trough, California, *in* Walawender, M.J., and Hanan, B.B., eds., Geological Excursions in Southern California and Mexico: San Diego, California, Department of Geological Sciences, San Diego State University, p. 397–416.

Kirby, S.M., 2005, The Quaternary Structural and Tectonic Evolution of the San Felipe Hills, CA. [M.S. thesis]: Logan, Utah, Utah State University, 3 plates, 181 p.

Kirby, S.M., Janecke, S.U., Dorsey, R.J., Housen, B.A., Langenheim, V., McDougall, K., and Steely, A.N., 2007, Pleistocene Brawley and Ocotillo Formations: Evidence for initial strike-slip deformation along the San Felipe and San Jacinto fault zones, southern California: The Journal of Geology, v. 115, p. 43–62, doi: 10.1086/509248.

Lizarralde, D., Axen, G.J., Brown, H.E., Fletcher, J.M., Antonio González-Fernández, A., Harding, A.J., Holbrook, W.S., Kent, G.M., Paramo, P., Sutherland, F., and Umhoefer, P.J., 2007, Variation in styles of rifting in the Gulf of California: Nature, v. 448, p. 466–469, doi: 10.1038/nature06035.

Lourens, L.J., Antonarakou, A., Hilgen, F.J., Van Hoof, A.A.M., Vergnaud-Grazzini, C., and Zachariasse, W.J., 1996, Evaluation of the Plio-Pleistocene astronomical timescale: Paleoceanography, v. 11, p. 391–413, doi: 10.1029/96PA01125.

Ludwig, K.R., 2001, SQUID 1.02; A User's Manual: Berkeley Geochronology Center Special Publication 2, 22 p.

Ludwig, K.R., 2003, User's Manual for Isoplot/Ex, Version 3.0; A Geochronological Toolkit for Microsoft Excel: Berkeley Geochronology Center Special Publication 4, 70 p.

Luther, A., Axen, G., Stockli, D., Kelley, S., and Grove, M., 2008, Preliminary apatite (U-Th)/He thermochronology of the eastern Santa Rosa and San Jacinto blocks, Peninsular Ranges, southern California: Geological Society of America Abstracts with Programs, v. 40, no. 6, p. 444.

Lutz, A.T., 2005, Tectonic Controls on Pleistocene Basin Evolution in the Central San Jacinto Fault Zone, Southern California [M.S. thesis]: Eugene, Oregon, University of Oregon, 136 p.

Lutz, A.T., Dorsey, R.J., Housen, B.A., and Janecke, S.U., 2006, Stratigraphic record of Pleistocene faulting and basin evolution in the Borrego Badlands, San Jacinto fault zone, southern California: Geological Society of America Bulletin, v. 118, p. 1377–1397, doi: 10.1130/B25946.1.

Machette, M.N., Personius, S.F., Nelson, A.R., Schwartz, D.P., and Lund, W.R., 1991, The Wasatch fault zone, Utah; segmentation and history of Holocene earthquakes: Journal of Structural Geology, v. 13, p. 137–149, doi: 10.1016/0191-8141(91)90062-N.

Machette, M.N., Personius, S.F., and Nelson, A.R., 1992, Paleoseismology of the Wasatch fault zone; summary, interpretations, conclusions, *in* Gori, P.L., and Hays, W.W., eds., Assessment of Earthquake Hazards and Risks along the Wasatch Front: U.S. Geological Survey Professional Paper P1500AJ, p. A1–A71.

Magistrale, H., and Rockwell, T.K., 1996, The central and southern Elsinore fault zone: Bulletin of the Seismological Society of America, v. 86, p. 1793–1803.

Mann, P., 2007, Global catalogue, classification and tectonic origins of restraining and releasing bends on active and ancient strike- slip fault systems, *in* Cunningham, W.D., and Mann, P., eds., Tectonics of Strike- Slip Restraining and Releasing Bends: Geological Society of London Special Publication 290, p. 13–142.

Mann, P., Hempton, M., Bradley, D., and Burke, K., 1983, Development of pull-apart basins: The Journal of Geology, v. 91, p. 529–554, doi: 10.1086/628803.

Matti, J.C., and Morton, D.M., 1993, Paleogeographic evolution of the San Andreas fault in southern California: A reconstruction based on a new cross-fault correlation, *in* Powell, R.E., Weldon, R.J., and Matti, J.C., eds., The San Andreas Fault System: Displacement, Palinspastic Reconstruction, and Geologic Evolution: Geological Society of America Memoir 178, p. 107–159.

Matti, J.C., Cox, B., Morton, D.M., Sharp, R.V., and King, T., 2002, Fault-bounded Neogene sedimentary deposits in the Santa Rosa Mountains, southern California; crustal stretching or transpressional uplift?: Geological Society of America Abstracts with Programs, v. 34, no. 6, p. 124.

May, S.R., Ehman, K.D., Gray, G., and Crowell, J.C., 1993, A new angle on the tectonic evolution of the Ridge Basin, a strike- slip basin, southern California: Geological Society of America Bulletin, v. 105, p. 1357–1372, doi: 10.1130/0016-7606(1993)105<1357:ANAOTT>2.3.CO;2.

McCalpin, J.P., and Nishenko, S.P., 1996, Holocene paleoseismicity, temporal clustering, and probabilities of future large (M>7) earthquakes on the Wasatch fault zone, Utah: Journal of Geophysical Research, v. 101, p. 6233–6253, doi: 10.1029/95JB02851.

McDougall, K., 2008, Late Neogene marine incursions and the ancestral Gulf of California, *in* Reheis, M., Herschler, R., and Miller, D., eds., Late Cenozoic Drainage History of the Southwestern Great Basin and Lower Colorado River Region: Geologic and Biotic Perspectives: Geological Society of America Special Paper 439, p. 355–373.

McDougall, K.A., Poore, R.Z., and Matti, J.C., 1999, Age and paleoenvironment of the Imperial Formation near San Gorgonio Pass, southern California: Journal of Foraminiferal Research, v. 29, p. 4–25.

McKenzie, D.P., 1978, Some remarks on the development of sedimentary basins: Earth and Planetary Science Letters, v. 40, p. 25–32.

Miller, K.G., Kominz, M.A., Browning, J.V., Wright, J.D., Mountain, G.S., Katz, M.E., Sugarman, P.J., Cramer, B.S., Christie-Blick, N., and Pekar, S.F., 2005, The Phanerozoic record of global sea-level change: Science, v. 310, p. 1293–1298, doi: 10.1126/science.1116412.

Moucha, R., Forte, A.M., Mitrovica, J.X., Rowley, D.B., Quéré, S., Simmons, N.A., and Grand, S.P., 2008, Dynamic topography and long-term sea-level variations: There is no such thing as a stable continental platform: Earth and Planetary Science Letters, v. 271, p. 101–108, doi: 10.1016/j.epsl.2008.03.056.

Muffler, J.L.P., and White, D.E., 1969, Active metamorphism of the upper Cenozoic sediments in the Salton Sea geothermal field and the Salton Trough, southern California: Geological Society of America Bulletin, v. 80, p. 157–182, doi: 10.1130/0016-7606(1969)80[157:AMOUCS]2.0.CO;2.

Muto, T., and Steel, R.J., 1992, Retreat of the front in a prograding delta: Geology, v. 20, p. 967–970, doi: 10.1130/0091-7613(1992)020<0967:ROTFIA>2.3.CO;2.

Muto, T., and Steel, R.J., 2001, Auto-stepping during the transgressive growth of deltas: Results from flume experiments: Geology, v. 29, p. 771–774, doi: 10.1130/0091-7613(2001)029<0771:ADTTGO>2.0.CO;2.

Muto, T., and Steel, R.J., 2002, In defense of shelf-edge delta development during falling and lowstand of relative sea level: The Journal of Geology, v. 110, p. 421–436, doi: 10.1086/340631.

Nicholson, C., Sorlien, C.C., Atwater, T., Crowell, J.C., and Luyendyk, B.P., 1994, Microplate capture, rotation of the western Transverse Ranges, and initiation of the San Andreas transform as a low-angle fault system: Geology, v. 22, p. 491–495, doi: 10.1130/0091-7613(1994)022<0491:MCROTW>2.3.CO;2.

Opdyke, N.D., Lindsay, E.H., Johnson, N.M., and Downs, T., 1977, The paleomagnetism and magnetic polarity stratigraphy of the mammal-bearing section of Anza Borrego State Park, California: Quaternary Research, v. 7, p. 316–329, doi: 10.1016/0033-5894(77)90024-2.

Oskin, M., and Stock, J.M., 2003a, Marine incursion synchronous with plate-boundary localization in the Gulf of California: Geology, v. 31, p. 23–26, doi: 10.1130/0091-7613(2003)031<0023:MISWPB>2.0.CO;2.

Oskin, M., and Stock, J.M., 2003b, Pacific–North America plate motion and opening of the Upper Delfín basin, northern Gulf of California: Geological Society of America Bulletin, v. 115, p. 1173–1190, doi: 10.1130/B25154.1.

Oskin, M., Stock, J., and Martín-Barajas, A., 2001, Rapid localization of Pacific–North America plate motion in the Gulf of California: Geology, v. 29, p. 459–462, doi: 10.1130/0091-7613(2001)029<0459:RLOPNA>2.0.CO;2.

Paola, C., Heller, P.L., and Angevine, C.L., 1992, The large-scale dynamics of grain-size variation in alluvial basins; 1. Theory: Basin Research, v. 4, p. 73–90.

Persaud, P., Stock, J.M., Steckler, M.S., Martin-Barajas, A., Diebold, J.B., Gonzalez-Fernandez, A., and Mountain, G.S., 2003, Active deformation and shallow structure of the Wagner, Consag, and Delfin basins, northern Gulf of California, Mexico: Journal of Geophysical Research, v. 108, doi: 10.1029/2002JB001937.

Pinault, C.T., 1984, Structure, Tectonic Geomorphology and Neotectonics of the Elsinore Fault Zone between Banner Canyon and the Coyote Mountains, Southern California [M.S. thesis]; San Diego, California, San Diego State University, 231 p.

Pitman, W.C., and Andrews, J.A., 1985, Subsidence and thermal history of small pull- apart basins, *in* Biddle, K.T., and Christie-Blick, N., eds., Strike-Slip Deformation, Basin Formation, and Sedimentation: Society of Economic Paleontologists and Mineralogists Special Publication 37, p. 45–50.

Porebski, S.J., and Steel, R.J., 2006, Deltas and sea-level change: Journal of Sedimentary Research, v. 76, p. 390–403, doi: 10.2110/jsr.2006.034.

Posamentier, H.W., Jervey, M.T., and Vail, P.R., 1988, Eustatic controls on clastic deposition: I. Conceptual framework, *in* Wilgus, C.K., Hastings, B.S., Kendall, C.G.St.C., Posamentier, H.W., Ross, C.A., and Van Wagoner, J.C., eds., Sea-Level Changes: An Integrated Approach: Society of Economic Paleontologists and Mineralogists Special Publication 42, p. 109–124.

Powell, R.E., 1981, Geology of the Crystalline Basement Complex, Eastern Transverse Ranges, Southern California: Constraints on Regional Tectonic Interpretation [Ph.D. thesis]: Pasadena, California, California Institute of Technology, 441 p.

Powell, R.E., 1993, Balanced palinspastic reconstruction of pre–late Cenozoic paleogeology, southern California: Geologic and kinematic constraints on evolution of the San Andreas fault system, *in* Powell, R.E., Weldon, R.J., and Matti, J.C., eds., The San Andreas Fault

System: Displacement, Palinspastic Reconstruction, and Geologic Evolution: Geological Society of America Memoir 178, p. 1–106.

Powell, R.E., and Weldon, R.J., II, 1992, Evolution of the San Andreas fault: Annual Review of Earth and Planetary Sciences, v. 20, p. 431–468, doi: 10.1146/annurev.ea.20.050192.002243.

Ruisaard, C.I., 1979, Stratigraphy of the Miocene Alverson Formation, Imperial County, California [M.S. Thesis]: San Diego, California, San Diego State University, 125 p.

Rymer, M.J., Sarna-Wojcicki, A.M., Powell, C.L., and Barron, J.A., 1994, Stratigraphic evidence for late Miocene opening of the Salton Trough in southern California: Geological Society of America Abstracts with Programs, v. 26, no. 2, p. 87.

Rymer, M.J., Powell, C.L., Sarna-Wojcicki, A.M., II, and Barron, J.A., 1995, Late Miocene stratigraphic and paleogeographic setting of Garnet Hill in the northwestern Salton Trough, Southern California: American Association of Petroleum Geologists (AAPG) Pacific Section Meeting Abstracts, v. 79, no. 4, p. 596.

Sarna-Wojcicki, A.M., Bowman, H.R., Meyer, C.E., Russell, P.C., Woodward, M.J., McCoy, G., Rowe, J.J., Jr., Baedecker, P.A., Asarao, F., and Michael, H., 1984, Chemical Analyses, Correlations, and Ages of Upper Pliocene and Pleistocene Ash Layers of East-Central and Southern California: U.S. Geological Survey Professional Paper 1293, 40 p.

Sarna-Wojcicki, A.M., Meyer, C.E., Wan, E., and Soles, S., 1997, Age and correlation of tephra layers, position of the Matuyama-Brunhes chron boundary, and effects of Bishop ash eruption on Owens Lake, as determined from drill core OL-92, southeast California, *in* Smith, G.I., and Bischoff, J.L., eds., An 800,000-Year Paleoclimatic Record from Core OL-92, Owens Lake, Southeast California: Geological Society of America Special Paper 317, p. 79–90.

Sarna-Wojcicki, A.M., Reheis, M.C., Pringle, M.S., Fleck, R.J., Burbank, D., Meyer, C.E., Slate, J.L., Wan, E., Budahn, J.R., Troxel, B., and Walker, J.P., 2005, Tephra Layers of Blind Spring Valley and Related Upper Pliocene and Pleistocene Tephra Layers, California, Nevada, and Utah: Isotopic Ages, Correlation, and Magnetostratigraphy: U.S. Geological Survey Professional Paper 1701, 63 p.

Schärer, U., 1984, The effect of initial ^{230}Th disequilibrium on young U-Pb ages: The Makalu case, Himalaya: Earth and Planetary Science Letters, v. 67, p. 191–204, doi: 10.1016/0012-821X(84)90114-6.

Schmitt, A.K., and Vazquez, J.A., 2006, Alteration and remelting of nascent oceanic crust during continental rupture: Evidence from zircon geochemistry of rhyolites and xenoliths from the Salton Trough, California: Earth and Planetary Science Letters, v. 252, p. 260–274, doi: 10.1016/j.epsl.2006.09.041.

Schmitz, M.D., and Bowring, S.A., 2001, U-Pb zircon and titanite systematics of the Fish Canyon Tuff: An assessment of high-precision U-Pb geochronology and its application to young volcanic rocks: Geochimica et Cosmochimica Acta, v. 65, no. 15, p. 2571–2587, doi: 10.1016/S0016-7037(01)00616-0.

Sclater, J.G., and Christie, P.A.F., 1980, Continental stretching: An explanation of the post–Mid-Cretaceous subsidence of the Central North Sea Basin: Journal of Geophysical Research, v. 85, no. B7, p. 3711–3739, doi: 10.1029/JB085iB07p03711.

Seeber, L., Sorlien, C., Steckler, M., and Cormier, M.H., 2010, Continental transform basins: Why are they asymmetric?: Eos, v. 91, no. 4, p. 29–30, doi: 10.1029/2010EO040001.

Severinghaus, J., and Atwater, T.M., 1990, Cenozoic geometry and thermal state of the subducting slabs beneath North America, *in* Wernicke, B.P., ed., Basin and Range Extensional Tectonics Near the Latitude of Las Vegas: Geological Society of America Memoir 176, p. 1–22.

Sharp, R.V., 1967, San Jacinto fault zone in the Peninsular Ranges of southern California: Geological Society of America Bulletin, v. 78, p. 705–729, doi: 10.1130/0016-7606(1967)78[705:SJFZIT]2.0.CO;2.

Shirvell, C., 2006, Pliocene Exhumation along the West Salton Detachment System and Tectonic Evolution of the Fish Creek–Vallecito Supradetachment Basin, Salton Trough, Southern California [M.S. thesis]: Los Angeles, University of California, 133 p.

Shirvell, C.R., Stockli, D.F., Axen, G.J., and Grove, M., 2009, Miocene-Pliocene exhumation along the west Salton detachment fault, southern California, from (U-Th)/He thermochronometry of apatite and zircon: Tectonics, v. 28, p. TC2006, doi: 10.1029/2007TC002172.

Spasojevic, S., Liu, L., Gurnis, M., and Müller, R.D., 2008, The case for dynamic subsidence of the U.S. East Coast since the Eocene: Geophysical Research Letters, v. 35, p. L08305, doi: 10.1029/2008GL033511.

Spencer, J.E., and Normark, W.R., 1979, Tosco-Abreojos fault zone: A Neogene transform plate boundary within the Pacific margin of southern Baja California: Geology, v. 7, p. 554–557, doi: 10.1130/0091-7613(1979)7<554:TFZANT>2.0.CO;2.

Steely, A.N., 2006, The Evolution from Late Miocene West Salton Detachment Faulting to Cross-Cutting Pleistocene Oblique Strike Slip Faults in the SW Salton Trough, Southern California [M.S. thesis]: Logan, Utah, Utah State University, 3 plates, 238 p.

Steely, A.N., Janecke, S.U., Dorsey, R.J., and Axen, G.J., 2009, Early Pleistocene initiation of the San Felipe fault zone, SW Salton Trough, during reorganization of the San Andreas fault system: Geological Society of America Bulletin, v. 121, p. 663–687, doi: 10.1130/B26239.1.

Steiger, R.H., and Jäger, E., 1977, Subcommission on Geochronology: Convention on the use of decay constants in geo- and cosmochronology: Earth and Planetary Science Letters, v. 36, p. 359–362, doi: 10.1016/0012-821X(77)90060-7.

Stock, J.M., and Hodges, K.V., 1989, Pre-Pliocene extension around the Gulf of California and the transfer of Baja California to the Pacific plate: Tectonics, v. 8, p. 99–115, doi: 10.1029/TC008i001p00099.

Tera, F., and Wasserburg, G., 1972, U-Th-Pb systematics in three *Apollo 14* basalts and the problem of initial Pb in lunar rocks: Earth and Planetary Science Letters, v. 14, p. 281–304, doi: 10.1016/0012-821X(72)90128-8.

Todd, V.R., 2004, Preliminary Geologic Map of the El Cajon 30′ × 60′ Quadrangle, Southern California, Version 1.0: U.S. Geological Survey Open-File Report 2004–1361, scale 1:100,000.

van der Woerd, J., Klinger, Y., Sieh, K., Tapponnier, P., Ryerson, F.J., and Mériaux, A.S., 2006, Long-term slip rate of the southern San Andreas fault from 10 Be–26 Al surface exposure dating of an offset alluvial fan: Journal of Geophysical Research, v. 111, p. B04407, doi: 10.1029/2004JB003559.

Van Hinte, J.E., 1978, Geohistory analysis—Application of micropaleontology in exploration geology: American Association of Petroleum Geologists Bulletin, v. 62, p. 201–222.

Van Sickel, W.A., Kominz, M.A., Miller, K.G., and Browning, J.V., 2004, Late Cretaceous and Cenozoic sea-level estimates: Backstripping analysis of borehole data, onshore New Jersey: Basin Research, v. 16, p. 451–465, doi: 10.1111/j.1365-2117.2004.00242.x.

Van Wagoner, J.C., Mitchum, R.M., Campion, K.M., and Rahmanian, V.D., 1990, Siliciclastic Sequence Stratigraphy in Well Logs, Cores, and Outcrops: Concepts for High-Resolution Correlation of Time and Facies: American Association of Petroleum Geologists, Methods in Exploration Series 7, 55 p.

Weldon, R.J., II, Meisling, K.E., and Alexander, J., 1993, A speculative history of the San Andreas fault in the central Transverse Ranges, California, *in* Powell, R.E., Weldon, R.J., II, and Matti, J.C., eds., The San Andreas Fault System: Displacement, Palinspastic Reconstruction, and Geologic Evolution: Geological Society of America Memoir 178, p. 161–198.

Williams, I.S., 1998, U-Th-Pb geochronology by ion microprobe, *in* McKibben, M.A., Shanks III, W.C., and Ridley, W.I., eds., Applications of Microanalytical Techniques to Understanding Mineralizing Processes: Reviews in Economic Geology, v. 7, p. 1–35.

Wilson, D.S., McCrory, P.A., and Stanley, R.G., 2005, Implications of volcanism in coastal California for the Neogene deformation history of western North America: Tectonics, v. 24, p. TC3008, doi: 10.1029/2003TC001621.

Winker, C.D., 1987, Neogene Stratigraphy of the Fish Creek–Vallecito section, Southern California: Implications for Early History of the Northern Gulf of California and the Colorado Delta [Ph.D. thesis]: Tucson, University of Arizona, 494 p.

Winker, C.D., and Kidwell, S.M., 1986, Paleocurrent evidence for lateral displacement of the Pliocene Colorado River delta by the San Andreas fault system, southeastern: California Geology, v. 14, p. 788–791.

Winker, C.D., and Kidwell, S.M., 1996, Stratigraphy of a marine rift basin: Neogene of the western Salton Trough, California, *in* Abbott, P.L., and Cooper, J.D., eds., Field Conference Guidebook and Volume for the American Association of Petroleum Geologists Annual Convention: American Association of Petroleum Geologists: Bakersfield, California, p. 295–336.

Woodard, G.D., 1963, The Cenozoic Succession of the West Colorado Desert, San Diego and Imperial Counties, Southern California [Ph.D. thesis]: Berkeley, University of California, 494 p.

Woodard, G.D., 1974, Redefinition of Cenozoic stratigraphic column in Split Mountain Gorge, Imperial Valley, California: The American Association of Petroleum Geologists Bulletin, v. 58, p. 521–539.

Xie, X., and Heller, P.L., 2009, Plate tectonics and basin subsidence history: Geological Society of America Bulletin, v. 121, p. 55–64.

Manuscript Received 3 September 2009
Revised Manuscript Received 17 March 2010
Manuscript Accepted 18 March 2010

Printed in the USA